INTELLECTUAL PROPERTY INDIA
PATENTS | DESIGNS | TRADE MARKS
GEOGRAPHICAL INDICATIONS

सत्यमेव जयते

क्रमांक : 044122358
SL No :

भारत सरकार
GOVERNMENT OF INDIA
पेटेंट कार्यालय
THE PATENT OFFICE

पेटेंट प्रमाणपत्र
PATENT CERTIFICATE

(Rule 74 Of The Patents Rules)

पेटेंट सं. / Patent No.	:	345596
आवेदन सं. / Application No.	:	6907/CHE/2015
फाइल करने की तारीख / Date of Filing	:	14/12/2015
पेटेंटी / Patentee	:	INDIAN INSTITUTE OF TECHNOLOGY MADRAS (IIT Madras)

प्रमाणित किया जाता है कि पेटेंटी को उपरोक्त आवेदन में यथाप्रकटित METHOD OF MAKING ALLOYS OF PRECISE COMPOSITION USING INTER-CLUSTER REACTIONS IN SOLUTION नामक आविष्कार के लिए, पेटेंट अधिनियम, १९७० के उपबंधों के अनुसार आज तारीख 14th day of December 2015 से बीस वर्ष की अवधि के लिए पेटेंट अनुदत्त किया गया है।

It is hereby certified that a patent has been granted to the patentee for an invention entitled METHOD OF MAKING ALLOYS OF PRECISE COMPOSITION USING INTER-CLUSTER REACTIONS IN SOLUTION as disclosed in the above mentioned application for the term of 20 years from the 14th day of December 2015 in accordance with the provisions of the Patents Act,1970.

एकस्य कार्यालय THE PATENT OFFICE GOVT.OF INDIA भारत सरकार

अनुदान की तारीख :
Date of Grant : 29/08/2020

पेटेंट नियंत्रक
Controller of Patent

टिप्पणी - इस पेटेंट के नवीकरण के लिए फीस, यदि इसे बनाए रखा जाना है, **14th day of December 2017** को और उसके पश्चात प्रत्येक वर्ष मे उसी दिन देय होगी।

Note. - The fees for renewal of this patent, if it is to be maintained will fall / has fallen due on 14th day of December 2017 and on the same day in every year thereafter.

FORM 2

THE PATENTS ACT, 1970

(39 OF 1970)

&

The Patents Rules, 2003

COMPLETE SPECIFICATION

(Refer section 10 and rule 13)

TITLE OF THE INVENTION:

METHOD OF MAKING ALLOYS OF PRECISE COMPOSITION USING INTER-CLUSTER REACTIONS IN SOLUTION

2. APPLICANT:

(A) NAME: **INDIAN INSTITUTE OF TECHNOLOGY MADRAS**

(B) NATIONALITY: Indian

(C) ADDRESS: **INDIAN INSTITUTE OF TECHNOLOGY MADRAS**

IIT P.O

Chennai - 600 036

3. Preamble to the Description

COMPLETE SPECIFICATION

The following specification particularly describes the invention and the manner in which is to be performed.

COMPLETE SPECIFICATION

TITLE OF THE INVENTION

METHOD OF MAKING ALLOYS OF PRECISE COMPOSITION USING INTER-CLUSTER REACTIONS IN SOLUTION

FIELD OF THE INVENTION

The present invention relates to inter-cluster chemistry for creating new alloys by solution state reactions of nanoclusters, in particular, monolayer protected noble metal clusters.

BACKGROUND OF THE INVENTION

Inter-cluster reactions between metal clusters are rare and their chemistry is mostly explored through reactions with small molecules [Kappes, M. M. *Chem. Rev.* 1988, *88*, 369, Schmid, G. *Chem. Rev.* 1992, *92*, 1709, Moskovits, M. *Annu. Rev. Phys. Chem.* 1991, *42*, 465, Luo, Z.; Gamboa, G. U.; Smith, J. C.; Reber, A. C.; Reveles, J. U.; Khanna, S. N.; Castleman, A. W. Jr. *J. Am. Chem. Soc.* 2012, *134*, 18973]. Monolayer protection with suitable ligands facilitated the synthesis of highly stable, atomically precise metal clusters in sufficient quantities [Heaven, M. W. et al., *J. Am. Chem. Soc.* 2008, *130*, 3754, Akola, J. et al. *J. Am. Chem. Soc.* 2008, *130*, 3756, Jadzinsky, P. D. et al., *Science* 2007, *318*, 430, Desireddy, A. et al., *Nature* 2013, *501*, 399]. This opened up a way to develop an in-depth understanding of their chemistry, conveniently in the solution phase. Reactions of these clusters in solutions are expected to complement the results obtained from gas phase experiments, providing further insights into their properties. Moreover, cluster chemistry in solution has practical applications [Yu, C. et al., *J. Phys. Chem. Lett.* 2013, *4*, 2847**,** Oliver-Meseguer, J. et al., *Science* 2012, *338*, 1452, Kwak, K., et al., *ACS Nano* 2014, *8*, 671] Among the ligand-protected metal clusters, thiolate-protected noble metal clusters ($Au_{25}(SR)_{18}$, for example) have been recognized as a distinct category in view of their unique properties [Jin, R. *Nanoscale* **2010**, *2*, 343, Udayabhaskararao, T. et al., *J. Phys. Chem. Lett.* 2013, *4*, 1553, Mathew, A. et al. *Part. Part. Syst. Charact.* 2014, *31*, 1017]

The earliest of the chemistry of these clusters has been ligand exchange [Song, Y.et al. *J. Am. Chem. Soc.* 2002, *124*, 7096, Parker, J. F. et al. *J. Phys. Chem. C* 2010, *114*, 8276, Dass, A. et al. *J. Phys. Chem. C* 2008, *112*, 20276, Shibu, E. S. et al. *J. Phys. Chem. C* 2008, *112,* 12168, Fernando, A. et al. *J. Phys. Chem. C* 2015, *119*, 20179] leading to an understanding of the localization of electronic transitions to the Au_nS_m moiety and demonstration of fluorescence resonance energy transfer (FRET) [Muhammed, M. A. H.et al. *J. Phys. Chem. C* 2008, *112*, 14324]. Though there have been a few attempts dealing with the reactions of these clusters with halocarbons [Bootharaju, M. S.et al. *J. Mater. Chem. A* 2013, *1*, 611], metal ions [Bootharaju, M. S. et al. *Langmuir*, 2011, *27*, 8134, Krishnadas, K. R. et al. *Eur. J. Inorg. Chem.* 2014, *5*, 908, Udayabhaskararao, T. et al. *Angew. Chem. Int. Ed.* 2012, *51*, 2155, Choi, J.-P. et al. *J. Phys. Chem. C* 2010, *114*, 15890, Wu, Z. *Angew. Chem. Int. Ed.* 2012, *51*, 2934], metal-thiolates [Wang, S.et al. *J. Am. Chem. Soc.* 2015, *137*, 4018], salts [Zhu, M.et al. *Nanoscale* 2011, *3*, 1703], and one-dimensional nanostructures [Som, A. et al. *Chem. Mater.* 2014, *26*, 3049], there has been no example of inter-cluster chemistry.

SUMMARY OF THE INVENTION

The present invention relates to inter-cluster chemistry for creating new alloys of precise composition by solution state reactions of nanoclusters, in particular, monolayer protected noble metal clusters.

Wherein the inter-cluster reactions occur between atomically precise, monolayer protected noble metal clusters using $Au_{25}(SR)_{18}$ and $Ag_{44}(SR)_{30}$ (RS- = alkyl/aryl thiolate) as model compounds.

In one embodiment, invention providing mass spectrometric measurements, both by electrospray ionization and matrix assisted laser desorption ionization, shows that the reaction occurs through the exchange of metal atoms and protecting ligands of the clusters.

In other embodiment, invention shows that inter-cluster alloying is a facile method for heteroatom doping by doping up to twenty Ag atoms into $Au_{25}(SR)_{18}$.

In yet another embodiment, invention depicts that the metal core-thiolate interfaces in these clusters play a crucial role in inducing these reactions and also affect rates of these reactions.

In another embodiment the invention shows that the newly formed alloys can have new properties such as an optical absorption (and consequently, luminescence) and have possibility to create new magnets, catalysts, etc.

DETAILED DESCRIPTION OF DRAWINGS

Figure 1 UV/Vis absorption and negative ion ESI MS spectra of $Au_{25}(PET)_{18}$ (A), $Ag_{44}(FTP)_{30}$ (B) and their 14:1 molar mixture (C) showing changes in the spectral features due to inter-cluster reaction. In A-C, panels a-c and a'-c' are the UV/Vis and ESI MS spectra, respectively. Characteristic peak positions are marked. Inset of a' shows the molecular ion region (m/z 7388-7400) of $Au_{25(}PET)_{18}$, showing isotope resolution. Inset of b' shows the same for $Ag_{44}(FTP)_{30}$ in the 3^- charge region (m/z 2848-2857). Theoretical (upper trace in inset of b′ and lower trace in inset of a′) and experimental (lower trace in inset of b′ and upper trace in inset of a′) spectra of ions are compared. The reaction product (marked in open rectangles) is expanded in the inset of c'. The corresponding clusters are also shown in between the spectra (modeled assuming the coordinates from the crystal structures). However, in the grayscale, the locations of atoms may not be distinguished clearly. Please refer to the Figure 33 for the labels. There are three types of Au atoms in $Au_{25}(SR)_{18}$ located at three symmetrically non-identical locations; namely, the centre of the icosahedron (labeled C), surface of icosahedrons (labeled I) and in the staples (labeled S). Similarly, there are four type of Ag atoms in $Ag_{44}(SR)_{30}$ located at four symmetrically non-identical locations; namely, surface of icosahedron (labeled I), in staples (S), on the face of the cube in the dodecahedron (labeled D_{cf}) and the vertices of the cube (labeled D_{cv}). Sulfur atoms of the thiolate ligands in these two clusters have been marked separately.

Figure 2 Negative ion mode MALDI MS spectra of the reaction mixtures for the $Au_{25}(PET)_{18}$:$Ag_{44}(FTP)_{30}$ ratio of (A) 14.0:1.0 (B) 7.0:1.0 and (C) 1.7:1.0. Each inset shows the expansion of the collection of peaks labeled I. The numbers (x, y) in parenthesis (in the insets), are according to the general molecular formula, $Au_{25-x}Ag_x(PET)_{18-y}(FTP)_y$. Shift in the centroids of group I with increase in concentration of $Ag_{44}(FTP)_{30}$ is marked with dotted lines.

Figure 3 Negative ion mode ESI MS spectra of the reaction mixtures for the $Au_{25}(PET)_{18}$:$Ag_{44}(FTP)_{30}$ ratio of (A) 14.0:1.0 (B) 7.0:1.0 and (C) 1.7:1.0. Each inset shows the expansion of features marked in open rectangles. The numbers (x, y) in parenthesis, are

according to the general molecular formula, $Au_{25-x}Ag_x(PET)_{18-y}(FTP)_y$. Each peak (x, y) has its own isotope pattern and overlap of these features complicate the spectrum.

Figure 4 Negative ion mode MALDI MS spectra showing the time-dependent changes in the reaction mixture of $Au_{25}(FTP)_{18}$ and $Ag_{44}(FTP)_{30}$ after 1h (A) and 3h (B) of the reaction. $[Au_{21}Ag_x(FTP)_{14}]$- are the fragments from the alloy clusters due to the loss of $Au_4(FTP)_4$. (Figure 6).

Figure 5 Negative ion mode ESI MS spectra measured immediately after mixing $Au_{25}(PET)_{18}$ with $Ag_{44}(FTP)_{30}$ in the Au_{25}:Ag_{44} ratio 14:1 (A) and 2.5:1.0 (B). The numbers (x,y) in parenthesis are according to the general molecular formula, $Au_{25-x}\ Ag_x(PET)_{18-y}(FTP)_y$.

Figure 6 Collision energy-dependent ESI MS spectra of $Au_{25}(PET)_{18}$. Loss of $Au_4(SR)_4$ unit resulting in $Au_{21}(SR)_{14}$ is the typical fragmentation mode of $Au_{25}(SR)_{18}$.[Parker, J. F. et al., *Acc. Chem. Res.* **2010**, *43*, 1289; Angel, L. A. et al., *ACS Nano* **2010**, *4*, 4691]

Figure 7 ESI MS spectrum of $Ag_{44}(FTP)_{30}$ shown in trace b' of Figure 1B. Lower m/z region in A is expanded in B to show the fragmentation of $[Ag_{44}(FTP)_{30}]_4^-$ to give $[Ag_{43}(FTP)_{28}]_3^-$. Such a fragmentation pattern is in accordance with previous reports [Desireddy, A. et al., *Nature* **2013**, *501*, 399; Harkness, K. M. *Nanoscale*, **2012**, *4*, 4269] Isotope distribution of $[Ag_{44}(FTP)_{30}]_4^-$ is shown in C. Species such as $[Ag_{45}(FTP)_{30}]_3^-$ and $[Ag_{46}(FTP)_{31}]_3^-$ were also detected which could be due to minor byproducts.

Figure 8 MALDI MS spectra showing the temporal evolution of the products formed after mixing of $Au_{25}(PET)_{18}$ and $Ag_{44}(FTP)_{30}$ clusters at Au_{25}:Ag_{44} ratio of 14:1. Traces a and b in (A) are the mass spectra of the reaction mixture immediately after mixing and after 1h of mixing, respectively. The group I in a and b are expanded in a' and b', respectively. The numbers in parenthesis, (x, y), are according to the general molecular formula, $Au_{25-x}Ag_x(PET)_{18-y}(FTP)_y$. Au_4SR_4 loss is a standard fragemntation pattern of $Au_{25}(SR)_{18}$ clusters (Figure 6).

Figure 9 MALDI MS spectra showing the temporal evolution of the products formed after mixing of $Au_{25}(PET)_{18}$ and $Ag_{44}(FTP)_{30}$ clusters at Au_{25}:Ag_{44} ratio of 1.7:1. Traces a and b in (A) are the mass spectra of the reaction mixture immediately after mixing and after 1h of mixing, respectively. The group I in a and b are expanded in a' and b', respectively. The numbers in parenthesis, (x, y), are according to the general molecular formula, $Au_{25-x}Ag_x(PET)_{18-y}(FTP)_y$. Au_4SR_4 loss is a standard fragemntation pattern of $Au_{25}(SR)_{18}$ clusters (Figure 6).

Figure 10 MALDI MS spectra showing the temporal evolution of the products formed after mixing of $Au_{25}(PET)_{18}$ and $Ag_{44}(FTP)_{30}$ clusters at Au_{25}:Ag_{44} ratio of 1.0:1.0. Traces a and b in (A) are the mass spectra of the reaction mixture immediately after mixing and after 1h of mixing, respectively. The group I in a and b are expanded in a' and b', respectively. The numbers in parenthesis, (x, y), are according to the general molecular formula, $Au_{25-x}Ag_x(PET)_{18-y}(FTP)_y$.

Figure 11 Panels A-D shows the expansion of features (0, 0-3), (1, 0-4), (2, 0-4) and (3, 0-4), (shown in Figure 3), respectively. The numbers, for example, (0, 0-3) is according to the general formula, $Au_{25-x}Agx(PET)_{18-y}(FTP)_y$.

Figure 12 Panels A-D shows the expansion of features (4, 1-5), (5, 1-5), (6, 3-8) and (7, 3-8), (shown in Figure 3) respectively. The numbers, for example, (4, 1-5) is according to the general formula, $Au_{25-x}Agx(PET)_{18-y}(FTP)_y$.

Figure 13 Panels A-D shows the expansion of features (8, 3-9), (9, 3-9), (10, 4-9) and (11, 4-9), (shown in Figure 3) respectively. The numbers, for example, (8, 3-9) is according to the general formula, $Au_{25-x}Ag_x(PET)_{18-y}(FTP)_y$.

Figure 14 Panels A and B shows the expansion of features (12, 4-9) and (13, 4-9), (shown in Figure 3) respectively. The numbers, for example, (12, 4-9) is according to the general formula, $Au_{25-x}Ag_x(PET)_{18-y}(FTP)_y$.

Figure 15 Expansion of the mass spectra in panel A of Figure 3.

Figure 16 Experimental (lower trace) and theoretical (upper trace) isotope distributions of (A) $Au_{23}Ag_2(PET)_{18}$, (B) $Au_{23}Ag_2(PET)_{17}(FTP)_1$, (C) $Au_{23}Ag_2(PET)_{16}(FTP)_2$ and (D) $Au_{23}Ag_2(PET)_{15}(FTP)_3$. These species corresponds to those labeled as (2, 0), (2, 1), (2, 2) and (2, 3), respectively in Figure 3A inset.

Figure 17 Time-dependent changes in the UV/Vis (A) and emission (B) spectra during the reaction between $Au_{25}(PET)_{18}$ and $Ag_{44}(FTP)_{30}$ clusters taken in the ratio (Au_{25}:Ag_{44}) of 14:1. Solvent used was dichloromethane.

Figure 18 Time-dependent UV/Vis spectra (A) and emission (B) spectra during the reaction between $Au_{25}(PET)_{18}$ and $Ag_{44}(FTP)_{30}$ clusters taken in the ratio (Au_{25}:Ag_{44}) of 7:1.

Figure 19 Time-dependent UV/Vis spectra (A) and emission (B) spectra during the reaction between $Au_{25}(PET)_{18}$ and $Ag_{44}(FTP)_{30}$ clusters taken in the ratio (Au_{25}:Ag_{44}) of 1.7:1.0.

Figure 20 Negative ion mode MALDI MS spectra of the $Au_{25-x}Ag_x(PET)_{18-y}(FTP)_y$ (x=0,1-13; y=0,1-8) product clusters formed at $Au_{25}(PET)_{18}$:$Ag_{44}(FTP)_{30}$ ratio of (A) 0.7:1 and (B)1:1.

Group I is expanded in the inset. The numbers (x, y) in parenthesis (in the insets), are according to the general molecular formula, $Au_{25-x}Ag_x(PET)_{18-y}(FTP)_y$.

Figure 21 ESI MS spectrum of the mixture of $Au_{25}(PET)_{18}$ and $Ag_{44}(FTP)_{30}$ (in Au_{25}:Ag_{44} ratio 1:1) measured 1h after mixing. Features labelled in panel A are expanded in panels B-E. The peak labels in B-E are given accordig to the peak maxima in each bunch. However, due to large number of Ag atoms and resulting isotopic width, featutres within these bunches are not resolved fully (unlike in the Figure 11 and 12).

Figure 22 Time-dependent UV/Vis spectra during the reaction between $Au_{25}(PET)_{18}$ and $Ag_{44}(FTP)_{30}$ clusters taken in the ratio (Au_{25}:Ag_{44}) of 1.0:1.0.

Figure 23 Time-dependent UV/Vis spectra during the reaction between $Au_{25}(PET)_{18}$ and $Ag_{44}(FTP)_{30}$ clusters taken in the ratio (Au_{25}:Ag_{44}) of 0.7:1.0.

Figure 24 MALDI MS of the $Au_{25}(FTP)_{18}$ clusters synthesized through ligand exchange of $Au_{25}(n\text{-}BuS)_{18}$ with 4-fluorothiophenol. Inset shows the UV/Vis spectrum of $Au_{25}(FTP)_{18}$.

Figure 25 Time-dependent changes in the MALDI MS spectra of the products formed during the reaction between $Au_{25}(FTP)_{18}$ and$Ag_{44}(FTP)_{30}$. The spectra for 1 h and 3 h are shown in the main manuscript (Figure 4). The spectrum for 24 h is shown in the Figure 26.

Figure 26 MALDI MS spectra of the clusters formed after 24 h (expansion of the group I in the top most panel, i.e., spectrum for 24 h, Figure 25) the reaction between $Au_{25}(FTP)_{18}$ and $Ag_{44}(FTP)_{30}$. The peaks labeled as (13, 12)', (12, 13)', etc., are due to the exchange of a single FTP ligand in (13, 12) and (12, 13) clusters with a single n-BuS ligand (mass difference between these peaks are 38 Da, MFTP-Mn-BuS). The numbers in parenthesis, (m, n), are according to the general molecular formula, $Au_mAg_n(FTP)_{18}$.

Figure 27 ESI MS spectra measured immediately after mixing $Au_{25}(PET)_{18}$ and $Ag_{44}(FTP)_{30}$ at a Au_{25}:Ag_{44} ratio of 1.7:1. The numbers (x, y) in parenthesis are according to the general molecular formula, $Au_{25-x}Ag_x(PET)_{18-y}(FTP)_y$.

Figure 28 Time-dependent changes of group II features appeared in the MALDI MS spectra during the reaction of $Ag_{44}(FTP)_{30}$ and $Au_{25}(PET)_{18}$. Groups II in Figure 25 are expanded here. A gradual shift of the peak maxima to migher m/z is seen.

Figure 29 ESI MS spectra showing the formation of $Au_xAg_{44-x}(FTP)_{30}$ during the reaction between $Au_{25}(FTP)_{18}$ and $Ag_{44}(FTP)_{30}$ at a Au_{25}:Ag_{44} ratio of 0.7:1.0. The peaks in between are

due to the n-Butanethiol-containing Au_xAg_{44-x} species as the latter could not be completely removed from $Au_{25}(FTP)_{18}$ (see Figure 26).

Figure 30 UV/Vis spectra of the reaction mixtures (after 1h of the reaction) at Au_{25}:Ag_{44} ratios of 14:1, 7:1, 1.7:1 (A) and 1:1 and 0.7:1 (B). At lower Ag_{44} concentrations (in A) the spectra resembles more with the previously reported spectra of $Au_{25-x}Ag_x(SR)_{18}$ [Yao, C. et al., *Nano Lett.* **2015**, *15*, 1281]. At higher concentrations of Ag_{44} (in B), the spectra resembles more with the previously reported spectra of $Au_xAg_{44-x}(SR)_{30}$ [Yang, H. et al., *Nat. Commun.* **2013**, *4*, 2422]

Figure 31 Negative ion mode MALDI MS spectra of the products formed immediately (A) and after 1h (B) of mixing $Au_{25}(n\text{-}BuS)_{18}$ and $Ag_{44}(FTP)_{30}$ clusters in dichloromethane. Group I in B is expanded in C. Group I are the molecular ion peak of the alloy clusters with mixed ligands formed during the reaction and the group I* are due to their fragments (due to $Au_4(SR)_4$ loss). Peaks due to BuS-FTP, Ag-Au and (Ag-FTP)-(Au-BuS) exchanges are labeled in C.

Figure 32 MALDI MS spectra of the products formed immediately after mixing $Au_{25}(PET)_{18}$ and $Ag_{44}(MBA)_{30}$ clusters. Peaks due to MBA-PET, Ag-Au and (Ag-MBA)-(Au-PET) exchanges are marked.

Figure 33 Structures of (A) $Au_{25}(SR)_{18}$ and (B) $Ag_{44}(SR)_{30}$ showing different types of Ag/Au atoms and Ag-S/Au-S bonds. There are three types of Au atoms in $Au_{25}(SR)_{18}$ located at three symmetrically non-identical locations; namely, the centre of the icosahedron (labeled C), surface of icosahedron (labeled I) and in the staples (labeled S). Similarly, there are four types of Ag atoms in $Ag_{44}(SR)_{30}$ located at four symmetrically non-identical locations; namely, surface of icosahedron (labeled I), in staples (S), on the cube face of the dodecahedron (labeled D_{cf}) and the vertices of the cube (labeled D_{cv}). However, in the grayscale, these locations may not be distinguished clearly. Sulfur atoms of the thiolate ligands in these two clusters have been marked separately. The labels F1-F4 correspond to different types of Ag-S/Au-S bonds. F1 involves the terminal ligand while the others involve the bridging ligand. In F3 the bridging ligand binds to the Ag atoms in the cube vertices of the dodecahedron (Dcv). In F4 the bridging ligand binds to the cube faces of dodecahedron (Dcf).

Figure 34 Borromean-Rings diagram of $Au_{25}(SMe)_{18}$. The rings formed by pairs of coplanar staples are shown as ellipses. Gold atoms are shown by dots and stars represent the SMe ligands whose positions are taken to be identical with their sulfur atom. The core Au atoms are

numbered from 1 to 12 and the staple atoms are numbered clockwise from end of the staple, from 1 to 5. The three perpendicular C2 axes are marked with the associated Cartesian axis direction in brackets. The staple directions are labeled by the six staple locants D1 to D6. Inset (i) shows a 3D visualization of the ring structure of the core and staples of $Au_{25}(SR)_{18}$ aspicule, with each (Au_8S_6)-ring consisting of two coplanar staples and the core atoms that are bonded to these staples. See the description of Figure 33 for the explanation of the location of gold and sulfur atoms in $Au_{25}(SR)_{18}$ [Natarajan, G et al., *J. Phys. Chem. C* 2015 DOI: 10.1021/acs.jpcc.5b08193]

Figure 35 Structure of $Ag_{44}(SR)_{30}$ showing the accessibility of the icosahedral core Ag atoms. The bonds marked with orange arrows when broken make the core atoms more exposed. See Figure 33 and its description for the positions of atoms.

Figure 36 Mass spectra showing the thiolate fragments of (A) $Ag_{44}(FTP)_{30}$ and (B) $Au_{25}(PET)_{18}$.

Figure 37 shows schematic representation of the reaction between $Ag(SR_2)_2$ anion and the staples of $Au_{25}(SR_1)_{18}$ resulting in exchange of (A) fragment F1 (B) fragment F2. Color codes of the atoms: dark yellow (Au), light yellow (S), blue (Ag). Au and sulfur atoms in the staple are numbered from 1 to 5 (red). Gold atom labeled as 6 is part of the icosahedral core. Atoms in the $Ag(SR_2)_2$ are labeled as 2′, 3′ and 4′ (blue). Structures in the intermediate steps are labeled I to VII. Comparison of structures I and V in (A) shows that the fragment F1 was exchanged between the staples and fragment. Comparison of structures III′ and VII shows that the fragment F2 was exchanged between the stpale and fragment.

Figure 38 shows schematic representation of the reaction between $Ag(SR_2)_2$ anion and the staples of $Au_{25}(SR_1)_{18}$ resulting in Ag/Au exchange. Color codes of the atoms: dark yellow (Au), light yellow (S), blue (Ag). Au and sulfur atoms in the staple are numbered from 1 to 5 (red). Atoms in the $Ag(SR_2)_2$ are labeled as 2′, 3′ and 4′ (blue). Comparison of the structures III″ and IX show that Au atom (4) is exchanged with Ag atom (2′).

DETAILED DESCRIPTION OF THE INVENTION

The present invention relates to inter-cluster chemistry for creating new alloys by solution state reactions of nanoclusters, in particular monolayer protected noble metal clusters.

Wherein the inter-cluster reactions occur between atomically precise, monolayer protected noble metal clusters using $Au_{25}(SR)_{18}$ and $Ag_{44}(SR)_{30}$ (RS- = alkyl/aryl thiolate) as model compounds.

In one embodiment, invention providing mass spectrometric measurements, both by electrospray ionization and matrix assisted laser desorption ionization showing that the reaction occurs through the exchange of metal atoms and protecting ligands of the clusters.

In other embodiment, invention shows inter-cluster alloying is a facile method for heteroatom doping by doping up to twenty Ag atoms into $Au_{25}(SR)_{18}$.

In yet another embodiment, invention depicts that the metal core-thiolate interfaces in these clusters play a crucial role in inducing these reactions and also affect rates of these reactions.

Metal core-thiolate clusters used here for inter-cluster reactions were prepared as follows: Materials: Chloroauric acid trihydrate ($HAuCl_4.3H_2O$) was purchased from Sigma Aldrich. Silver nitrate ($AgNO_3$) was purchased from RANKEM India. 2-phenylethanethiol (PET), n-butanethiol (n-BuSH), 4-fluorothiophenol (FTP), 4-meracptobenzoic acid (MBA), tetraoctylammonium bromide (TOAB), tetraphenylphosphonium bromide (PPh_4Br), sodium borohydride ($NaBH_4$) were purchased from Sigma Aldrich. All the solvents used (tetrahydrofuran (THF), methanol, hexane, dichloromethane (DCM) and dimethylformamide (DMF)) were of analytical grade.

Synthesis of clusters: $Au_{25}(PET)_{18}$ and $Au_{25}(BuS)_{18}$: 2 mL of 50 mM $HAuCl_4.3H_2O$ in THF was diluted to 7.5 mL using THF. About 65 mg of TOAB was added to this solution and stirred at 1500 rpm for 30 min at room temperature. Initial yellow color of the solution turned deep red during stirring. About 0.5 mmol of pure thiol was added at a stretch while stirring at the same speed. The deep red color slowly turned to yellow and eventually became colorless after about 45 min. After stirring further for 2 h, 2.5 mL of ice cold aqueous $NaBH_4$ (0.2 M) was added in one lot. The solution turned black immediately and stir-ring was continued for 5 h. The solution was rotary evaporated and precipitated with methanol, washed repeatedly with the same and dried.

$Au_{25}(FTP)_{18}$: 5 mg of $Au_{25}(n\text{-}BuS)_{18}$ was dissolved in 0.5 mL of toluene and 150 times (by weight) of pure 4-fluorothiophenol was added to it. The solution was heated at 50°C in an oil bath while stirring. After about 25 min, clusters were precipitated with hexane and collected by

centrifugation. This precipitate was washed with hexane, dissolved in DCM and centrifuged to remove thiolates. This cluster solution was vacuum dried and stored at 4°C.

$[PPh_4]_4[Ag_{44}(FTP)_{30}]$:The cluster was synthesized following a solid state route[Rao, T. U. B. et.al., *J. Am. Chem. Soc.* 2010, *132*, 16304]. 20 mg of $AgNO_3$ and 12 mg of PPh_4Br were ground thoroughly in an agate mortar and pestle for 5 min. About 76 µL of 4-fluorothiophenol was added to it in one shot and the mixture was ground for about 3 more minutes. Dry $NaBH_4$ (45 mg) was added and the mixture was ground till the pasty mass became brown in color. This was extracted with 7 mL of dichloromethane and kept undisturbed at room temperature till UV/Vis spectra showed all the characteristic features of the cluster. The clusters were purified adopting the same protocol used for $Au_{25}(SR)_{18}$. $Na_4[Ag_{44}(MBA)_{30}]$ was synthesized following a reported method [Desireddy, A. et al., *Nature* **2013**, *501*, 399] with slight modifications.

Inter-cluster reactions: Stock solutions of clusters were prepared in dichloromethane, except for $Ag_{44}(MBA)_{30}$ which was prepared in DMF. Required volumes of each of the stock solutions were added into 1 mL of dichloromethane at room temperature and the mixture was stirred with a pipette. It was not stirred magnetically. The reaction occurred immediately after mixing as observed from the immediate color changes and time-dependent MALDI MS and ESI MS measurements. All reactions were carried out at room temperature (~ 30°C).

Mass spectral measurements: Performed matrix assisted laser desorption ionization (MALDI) and electrospray ionization (ESI) mass spectrometry (MS) measurements. Applied Biosystems Voyager DEPro (MALDI) and Waters Synapt G2-Si (ESI and MALDI) mass spectrometers are used. ESI MS had a maximum resolution of 50,000 in the mass range of interest.

Computational Details: DFT as implemented in the real-space grid-based projector augmented wave (GPAW) package [Enkovaara, J. et al., *J. Phys. Condens. Matter.* **2010**, *22*, 253202]. Calculated the energy difference between the unexchanged cluster and a single Ag atom exchanged $[Au_{25}(SR)_{18}]^-$ and a single Au atom exchanged $[Ag_{44}(SR)_{30}]4^-$, for each of the isomers. The three symmetry-unique positions for the Ag atom in $[Au_{25}(SR)_{18}]1^-$ were the central atom (denoted by C), icosahedral vertex atom (I), and the staple gold atom (S). The four symmetry unique positions in $[Ag_{44}(SR)_{30}]4^-$ for the Au atom were the outermost shell in the middle dodecahedron (S), one of the eight cubic vertex positions (Dcv) and one of the twelve cube-face capping atoms (Dcf), and last, atoms in inner icosahedron (I) (Figure 33). Calculated the energy of the overall reaction for the case of a single metal atom exchange in each

combination of final substituent positions. Also calculated the energies of the substitution reactions of a single metal atom and single metal-ligand fragment, Ag and Ag-SR into $[Au_{25}(SR)_{18}]$, or, Au and Au-SR into $[Ag_{44}(SR)_{30}]4^-$ for each of the symmetry-unique positions mentioned above. To investigate the feasibility of electron transfer in this system, compared the relative energies of the HOMO and LUMO states, for both $[Au_{25}(SR)_{18}]^-$and $[Ag_{44}(SR)_{30}]4^-$, and their alloys.

Results and Discussion

Reactions between clusters having different ligands:

Initially the reaction between $Au_{25}(PET)_{18}$ and $Ag_{44}(FTP)_{30}$ which were prepared as described in the experimental section. PET and FTP are the ligands protecting Au_{25} and Ag_{44} clusters, respectively (Experimental Section). Appropriate volume of their stock solutions were added into a fixed volume of dichloromethane at room temperature (~30°C) (Experimental Section for details) to get defined concentrations of the reacting species. UV/Visible (UV/Vis) absorption features and electrospray ionization mass spectra (ESI MS) of the clusters before and immediately after (within 1 min) mixing are shown in Figure 1. The molecular ion peak of $Au_{25}(PET)_{18}$ at m/z 7391 is shown in trace a' of Figure 1A along with the expanded isotopiclly resolved molecular ion. Typical fragmentation pattern of $Au_{25}(PET)_{18}$ shown in (Figure 6) proves the identity of the cluster. Optical absorption spectrum of $Au_{25}(PET)_{18}$ shows characteristic peaks [Zhu, M. et al., *J. Am. Chem. Soc.* **2008**, *130*, 5883] at 796, 683, 552, 445 and 397 nm (trace a in Figure 1A). Similarly, $Ag_{44}(FTP)_{30}$ is characteristic in its optical absorption spectrum [Desireddy, A et al., *Nature* **2013**, *501*, 399, Bakr, O. M. et al., *Angew. Chem.* **2009**, *121*, 6035, Harkness, K. M. et al., *Nanoscale*, **2012**, *4*, 4269] (trace b, Figure 1B). $[Ag_{44}(FTP)_{30}]3^-$ was the prominent feature in the ESI MS of $Ag_{44}(SR)_{30}$ (trace b', Figure 1B). Isotope distributions of the prominent features of these clusters match well with the theoretical patterns as shown in the insets. For example, the spectrum in the m/z 7388-7400 window of $Au_{25}(PET)_{18}$ (inset of trace a' in Figure 1A) shows all the isotope features of the molecular ion. Detailed assignment of the spectrum in trace b' of Figure 1B is given in Figure 7. Absorption features of $Au_{25}(PET)_{18}$ changed significantly and those due to $Ag_{44}(FTP)_{30}$ were not observed at all upon mixing the two clusters (trace c in Figure 1C). Comparing the ESI MS spectra in Figure

1A-C, observed that a series of peaks at m/z lower than $Au_{25}(PET)_{18}$ appeared immediately after mixing. These changes in the absorption and mass spectral features confirm that the clusters react with each other spontaneously in solution. Time-dependent changes during the reaction at various Au_{25}:Ag_{44} ratios (Figures 8-10) show that a series of peaks at lower m/z than $Au_{25}(PET)_{18}$ (labeled as group I) and a broad feature at m/z higher than $Ag_{44}(FTP)_{30}$ (labeled as group II) appeared immediately after mixing the clusters. While a larger distribution of product peaks appeared in group I just after mixing, only 3-4 prominent peaks were observed after 10-15 min. The mass spectra after 1 h were similar to the spectra after 10-15 min, indicating that the reaction got equilibrated/completed in this timescale.

Reaction was studied at various Au_{25}:Ag_{44} ratios. MALDI MS spectra of these reaction mixtures after one hour of the reaction are shown in Figure 2. As the concentration of $Ag_{44}(FTP)_{30}$ was increased, the centroid of group I shifted continually towards lower m/z values. Simultaneously, intensity of group II increased. Peaks in group I of Figure 2 are expanded in the insets. Mass difference between these peaks is either m/z 89 or 99. The difference of m/z 89 is due to the loss of an Au atom (197 Da) from $Au_{25}(PET)_{18}$ and a simultaneous inclusion of an Ag (108 Da) atom into it from $Ag_{44}(FTP)_{30}$. Mass difference of m/z 99 is attributed to the loss of an Au-PET moiety (334 Da) and the inclusion of an Ag-FTP moiety (235 Da). Apart from these processes, there is a possibility for the exchange of ligands alone, i.e. FTP-PET exchanges. Because of the broadness of the MALDI MS peaks and small mass difference between FTP and PET ligands (10 Da), unambiguous confirmation of such exchange processes is not possible with MALDI MS measurements alone. Therefore, ESI MS measurements were carried out to reveal the details of the peaks in group I.

ESI MS of the reaction mixtures at various Au_{25}:Ag_{44} ratios are shown in Figure 3. Reaction products in the $Au_{25}(PET)_{18}$ region alone are shown here. Two features from each panel (marked in open rectangles) are expanded in the corresponding insets. Expanded features of the panels A-C are given in Figures 11-14. These data reveal that each feature in these panels is a bunch of peaks separated by m/z 10. For example, the feature (2, 0-4) in Figure 3A is a collection of (2, 0), (2, 1), (2, 2), (2, 3) and (2, 4) peaks. The first number in parenthesis of peak labels gives the number of Ag atoms exchanged. The second number gives the number of FTP ligands exchanged. MALDI MS measurements (Figure 2) indicated the presence of features separated by either m/z 89 or 99 and ESI MS measurements confirmed these features. For

example, the peaks (1, 0), (2, 0), (3, 0), etc. and (1, 2), (2, 2), (3, 2), etc.are separated by m/z 89 (Figure 15). Peaks such as (1, 1), (2, 2), (3, 3), etc. are separated by m/z 99. Mass difference of 89 is due to the Ag-Au exchange and the mass difference of 99 is due to (Au-PET)-(Ag-FTP) exchange, as mentioned earlier. Theoretical and experimental isotope patterns of peaks in the (2, 0-4) feature are shown in Figure 16 which further confirm inclusion of the FTP ligand into $Au_{25}(PET)_{18}$. Thus, ESI MS measurements unambiguously confirm that the group I peaks observed in MALDI MS are due to the Ag-Au and (Ag-FTP)-(Au-PET) exchanges betweeen $Au_{25}(PET)_{18}$ and $Ag_{44}(FTP)_{30}$. From Figure 3, it is clear that FTP-PET exchange is also occurring in $Au_{25}(PET)_{18}$ (the feature (0, 0-3) in Figure 3A and Figure 15), in addition to Ag-Au and (Ag-FTP)-(Au-PET) exchanges. However, total number of metal atoms and ligands were unchanged in the product clusters in group I. Hence, the series of peaks in group I have been assigned the general formula, $Au_{25-x}Ag_x(PET)_{18-y}(FTP)_y$. Larger the concentration of $Ag_{44}(FTP)_{30}$, the more and more Ag and FTP ligands are incorporated into $Au_{25}(PET)_{18}$. Inclusion of up to 1-5, 2-7 and 8-13 Ag atoms were observed for $Au_{25}(PET)_{18}$:$Ag_{44}(FTP)_{30}$ ratios of 14.0:1.0, 7.0:1.0 and 1.7:1.0, respectively. Insets of Figure 3 show that as the number of incorporated Ag atoms increases, peaks within a bunch becomes less resolved because of the isotope distribution of Ag. While distinct mass separations (of m/z 10) due to pure ligand exchange are seen in the reactions of clusters with differing ligands, these cannot be observed for clusters of the same ligands. Temporal changes in the absorption and luminescence spectra during reactions at various Au_{25}:Ag_{44} ratios are presented in Figures 17-19. Emission spectrum of $Au_{25}(PET)_{18}^-$ shows a peak at 720 nm and a hump at 800 nm as reported previously [Wu, Z. et al., *Nano Lett.* **2010,** *10*, 2568]. When $Ag_{44}(FTP)_{30}$ was added to $Au_{25}(PET)_{18}$, in all the cases (Figures S12-S14), there was an immediate decrease in intensity of these features. But, as time goes, intensity increased with a slight redshift of about 10 nm (for both features). These results confirm the formation of $Au_{25-x}Ag_x(PET)_{18-y}(FTP)_y$, bimetallic clusters with mixed ligands.

The maximum number of Ag incorporations observed so far in the case of mixed ligand- and all thiolate-protected Au_{25} clusters [Shichibu, Y. et al., *J. Phys. Chem. C* **2007**, *111*, 7845; Negishi, Y. et al., *Chem. Commun.* **2010**, *46*, 4713; Kumara, C. et al., *J. Phys. Chem. Lett.* **2014**, *5*, 461] is 13 and 11, respectively. In contrast to these reports, present invention observed Ag doping of up to 13-16 and 16-20 atoms into $Au_{25}(SR)_{18}$ at higher concentrations of $Ag_{44}(FTP)_{30}$ (Figures 20 and 21). Absorption spectra of these reaction mixtures are displayed in Figures 22

and 23, respectively. Thus, current experiments demonstrate for the first time that replacement of more than 13 Au with Ag is possible in Au_{25}. It is important to recall that Au-Ag system is miscible in the entire composition window. This indicates that the inter-cluster reaction is much more facile in comparison to the co-reduction methods to synthesize $Au_{25-x}Ag_x(SR)_{18}$ clusters.

Reaction between clusters having same ligands:

While the products of inter-cluster reactions have been assigned, complications arise due to the simultaneous exchange of the metal and the ligand. Definite confirmation of exchange is possible by using clusters containing the same ligands. For this purpose, the present invention prepared $Au_{25}(FTP)_{18}$. Reactions of $Au_{25}(FTP)_{18}$ with $Ag_{44}(FTP)_{30}$ unambiguously confirm the incorporation of Ag into $Au_{25}(SR)_{18}$. MALDI MS and UV/Vis spectra of $Au_{25}(FTP)_{18}$ clusters are shown in Figure 24. The MS and UV/Vis data confirm the identity of the cluster. Time-dependent changes in the MALDI MS spectra of a mixture of these clusters are given in Figure 25. The mass spectra in the group I region after 1 h and 3 h of reaction are shown in Figure 4. The mass difference of m/z 89 (M_{Au}-M_{Ag}) between the peaks in group I clearly confirms the formation of Au_{25}-$_xAg_x(FTP)_{18}$ clusters. This shows that Ag inclusion of 1-5 and 1-13 was observed after 1h and 3h of the reaction, respectively. After 24h of reaction, Ag inclusion of up to 17 atoms was observed (Figure 25 and 26). Analysis of the time-dependent MALDI MS data for clusters with same and different ligands (Figures 9-10 and 25) show that ligand shell on the clusters play an important role in controlling the reactivity. Comparison of group I in Figures 8-10 and 25 reveal that there is a drastic difference in rates of reactions between Au and Ag clusters depending on whether the same or different ligand is used to protect them. Time-dependent MALDI MS measurements show that irrespective of the concentrations of the reactant clusters, the reaction between $Au_{25}(PET)_{18}$ and $Ag_{44}(FTP)_{30}$ got completed/equilibrated within 10-15 min. In contrast, the reaction between $Au_{25}(FTP)_{18}$ and $Ag_{44}(FTP)_{30}$ continued for several hours (Figure 25). During the reaction between clusters with different ligands, the mass spectra show peaks arising from the inclusion of one to several Ag atoms, which in turn transform to only 3-4 prominent peaks after about ten minutes. But in the case of clusters having thesame ligands, only 1-6 Ag inclusions are observed in group I even after 1 h of the reaction. When the ligands are different, the inter-cluster reaction may be initiated by a fast (Au-SR)–(Ag-SR′) exchange step, starting the disruption of the thiolate staples. This in turn can make the clusters

unstable leading to the incorporation of Ag and ligands. Thus, the nature of the ligand shell on the reactant clusters play an important role in controlling the reactivity of the clusters.

The invention observed both metal and ligand incorporations in $Au_{25}(PET)_{18}$, and proceeded to develop an understanding of the sequence of events leading to the formation of $Au_{25-x}Ag_x(PET)_{18-y}(FTP)_y$ clusters. Observed that which of the events, FTP-PET, Ag-Au or (Ag-FTP)-(Au-PET) exchange, is the first step. For this, mass spectra of reaction mixtures were measured immediately after mixing the clusters. These measurements (Figure 5) show that the Ag-Au, (Ag-FTP)-(Au-PET) and FTP-PET exchanges occur even at the beginning of the reaction. Parent $Au_{25}(PET)_{18}$ also undergo FTP-PET exchange (the peak (0, 1) in Figure 5A and 5B). However, only one FTP-PET exchange was observed for $Au_{25}(PET)_{18}$ and its relative intensity remained almost the same even at about six-fold increase in the concentration of $Ag_{44}(FTP)_{30}$ (Figure 5A & B). These observations show that Ag-Au and (Ag-FTP)-(Au-PET) exchanges are much faster than pure FTP-PET exchange.

Occurrence of peaks with a separation of m/z 10, in the insets of Figure 3 and Figure 15, may be tempting to conclude that all of these clusters are formed through FTP-PET exchange. For example, the peaks (1, 1) to (1, 4) in Figure 15 may, at first, be considered as the products of sequential FTP-PET exchange of (1, 0) cluster. Mass spectral measurements immediately after mixing (Figure 5 and 27) the clusters reveal that this is not the case. Comparison of Figures 5A and 5B, shows that while the relative intensities of the (1, 0) and (1, 1) peaks significantly increases with concentration of $Ag_{44}(FTP)_{30}$, there is no such notable increase in the intensity of the (0, 1) peak. Also, as mentioned before, only one peak due to FTP-PET exchange of $Au_{25}(PET)_{18}$ was observed even when the concentration of $Ag_{44}(FTP)_{30}$ was increased about six times, i.e, no (0, 2) or (0, 3) peaks were observed even at higher concentration of Ag_{44}. These observations suggest that the clusters (1, 0) and (1, 1) are produced from (0, 0), i.e, the parent $Au_{25}(PET)_{18}$, through Ag-Au and (Ag-FTP)-(Au-PET) exchanges, respectively. For the same reasons, it is unlikely that the (1, 1) clusters is formed by a Ag-Au exchange of (0, 1) because the intensity of the latter is significantly less than that of (0, 0). Even though the clusters such as (1, 2) and (2, 3) are observed in the initial stages of reaction (Figure 5A & B), no (0, 2) and (0, 3) clusters were observed. Hence, the (1, 2) and (2, 3) clusters are more likely to be formed by FTP-PET exchange of (1, 1) and (2, 2) clusters and cannot be the result of Ag-Au exchange from (0, 2) and (0, 3) clusters. Thus, it can be concluded that the presence of FTP in the Au_{25}-

$_xAg_x(PET)_{18-y}(FTP)_y$ clusters formed is mostly due to (Ag-FTP)-(Au-PET) exchanges than due to FTP-PET exchanges.

These observations together suggest that $Au_{25-x}Ag_x(PET)_{18-y}(FTP)_y$ clusters were formed principally by two processes: (Ag-FTP)–(Au-PET) and Ag-Au exchanges. For example, the (1, 1) cluster (Figure 3 for numbering) is formed by the (Ag-FTP)-(Au-PET) exchange from a (0, 0) cluster. The (1, 1) cluster may then undergo Ag-Au or (Ag-FTP)-(Au-PET) exchange, producing (2, 1) or (2, 2) clusters, respectively. These processes continue to give higher Ag- and FTP-incorporated clusters. There may be other complicated events as well.

Transformation of $Au_{25}(SR)_{18}$ into $Au_{25-x}Ag_x(SR)_{18}$ is confirmed from the above measurements. Similarly, current measurements indicate that $Ag_{44}(SR)_{30}$ has been transformed into $Au_xAg_{44-x}(SR)_{30}$ due to its reaction with $Au_{25}(SR)_{18}$. As mentioned earlier, the mass spectral features due to $Ag_{44}(FTP)_{30}$ disappeared immediately after mixing it with $Au_{25}(PET)_{18}$. MALDI MS measurements show the emergence of a broad peak (group II) at m/z higher than that of $Ag_{44}(FTP)_{30}$ (Figures 2 and 20). Also the intensity of this peak increased as the concentration of $Ag_{44}(FTP)_{30}$ increased. The difference between the molecular mass of $Ag_{44}(FTP)_{30}$ (m/z 8567) and the maxima of group II peaks, at different time intervals (1-24 h) of the reaction between $Ag_{44}(FTP)_{30}$ and $Au_{25}(FTP)_{18}$, (Figure 28) suggests the formation of $Au_xAg_{44-x}(FTP)_{30}$ with x=14-16. However, such an analysis may not give accurate compositions of a mixture due to the high energy provided by the laser. ESI MS measurements (Figure 29) clearly indicated the formation of a series of clusters with x varying from 0-12. MALDI MS could not resolve the features of these individual clusters due to the broadness of the peaks. Recent reports on the $Au_xAg_{44-x}(SR)_{30}$ clusters[Yang, H et al., *Nat. Commun.* **2013**, *4*, 2422] (prepared from ionic precursors) indicate that the total number of metal atoms is the same and the structural framework of these clusters is similar to that of $Ag_{44}(SR)_{30}$. UV/Vis spectra of reaction mixtures at higher concentrations of Ag_{44} (Figure 30B) resemble that of previously reported $Au_{12}Ag_{32}(SR)_{30}$ clusters.[Yang, H. et al., *Nat. Commun.* **2013**, *4*, 2422] At lower Ag_{44} concentrations, (Figure 30A) the absorption spectra resemble $Au_{25-x}Ag_x(SR)_{18}$, as seen in previous reports.[Yao, C. et al., *Nano Lett.* **2015**, *15*, 1281] Hence, current MALDI and ESI MS measurements confirm the formation of $Au_xAg_{44-x}(SR)_{30}$ in the reaction between $Ag_{44}(FTP)_{30}$ and $Au_{25}(SR)_{18}$. Reactions were carried out with Au_{25} and Ag_{44} clusters of different protecting ligands (n-butanethiol and 4-meracptobenzoic acid) also (Figures 31 and 32). Present

experiments show that similar reactions occur between other types of Ag and Au clusters and even with plasmonic nanoparticles. Experiments are in progress in these directions. A discussion of the possible locations of Ag atoms in the alloy clusters, based on the charge states of $Au_{25}(SR)_{18}$, previous reports of $Au_{25-x}Ag_x$ clusters and the recent report of $Au_{25}Ag_2(SR)_{18}$,[Yao, C et al., *Nano Lett.* **2015**, *15*, 1281]. However, analysis of the structures formed requires more work.

To understand the driving force behind the reaction, the present invention used DFT to calculate energies of the reactants [$Au_{25}(SR)_{18}$ and $Ag_{44}(SR)_{30}$], the products [$Au_{25-x}Ag_x(SR)_{18}$ and $Au_xAg_{44-x}(SR)_{30}$] and the likely species being exchanged in the intermediate steps such as metal atoms (M), and thiolate fragments (M-SR) (Table 2-8). Calculated the energy of the overall reaction (i.e. $Au_{25}(SR)_{30} + Ag_{44}(SR)_{30} \rightarrow Au_{25-x}Ag_x(SR)_{18} + Au_xAg_{44-x}(SR)_{30}$) and reaction energies for substitution of metal atom (M=Ag/Au) and metal-thiolate fragments (M-SR) in different combinations of substituent positions in $Au_{25}(SR)_{18}$ and $Ag_{44}(SR)_{30}$, respectively (Table 1 and Tables 5-8). The overall reaction, either through M or M-SR substitutions, was found to be exothermic for certain combinations of substituent positions as shown in Table 1C. This can be attributed to the lowering of the total energy by inclusion of Au atoms or Au-SR into $Ag_{44}(SR)_{30}$ rather than the inclusion of Ag atom into $Au_{25}(SR)_{18}$ (Table 5-8). The more exothermic gold atom or fragment substitution into $Ag_{44}(SR)_{30}$ compensates for the endothermic [Walter, M et al., *J. Phys. Chem. C* **2009,** *113,* 15834] silver atom inclusion into the $Au_{25}(SR)_{18}$ in contrast to the exothermic Pd or Pt inclusion.[Negishi, Y. et al., *Phys. Chem. Chem. Phys.***2010**, *12*, 6219; Guidez, E. B. et al., *J. Phys. Chem. C***2012**, *116*, 20617] The details are discussed below.

The present invention investigated which substituent atom (M) or M-SR fragment positions in each cluster were most preferred energetically and the dependence of the reaction energy as a function of the final substituent positions. Initially calculated the energies of different isomers of $Au_{25-x}Ag_x(SR)_{18}$ and $Au_xAg_{44-x}(SR)_{30}$ for x=1, relative to the unalloyed clusters. For simplicity, considered events involving one metal atom substitution into $Au_{25}(SR)_{18}$ and $Ag_{44}(SR)_{30}$. There are a large number of symmetry non-equivalent isomers for each substitution; for eg., when x=2 there are 28 isomers for $Au_{25-x}Ag_x(SR)_{18}$) [Natarajan, G. et al., *J. Phys. Chem. C* 2015 DOI: 10.1021/acs.jpcc.5b08193] The preferred locations of substituent metal atoms or

fragments in the alloy clusters are indicated by the substitution energy differences between the parent clusters and their alloy isomers, listed in Table 1 A and B.

In case of $Au_{25-x}Ag_x(SR)_{18}$, Ag atoms prefer to stay on the icosahedral vertex positions (Table 3) as in earlier reports.[Kumara, C et al., *J. Phys. Chem. Lett.* **2014**, *5*, 461; Guidez, E. B. et al., *J. Phys. Chem. C* **2012**, *116*, 20617] For $Au_xAg_{44-x}(SR)_{30}$, the order of preference of the position of Au atom is the innermost icosahedron (-0.72 eV), followed by the outermost staple atoms (-0.48 eV), and last, the middle dodecahedral positions D_{cv} and D_{cf} (-0.14 and -0.32 eV) (Table 2). Reaction energies as a function of substituent positions for $Au_{25-x}(SR)_{18}$ and $Au_xAg_{44-x}(SR)_{30}$ in the alloy clusters (Table 1C) suggest that at fewer numbers of substituent metal atoms ($x \leq 12$), the most energetically favored final metal atom positions are in the icosahedral sites in both $Au_{25}(SR)_{18}$ and $Ag_{44}(SR)_{30}$ (-0.486 eV), and next, in the staples of one cluster and the icosahedral core of the other cluster (-0.245 and -0.276 eV). As mentioned earlier, the similarity of the absorption spectra of the reaction mixture at higher concentrations of $Ag_{44}(SR)_{30}$ (Figure 30B) with the previously reported $Au_{12}Ag_{32}(SR)_{30}$ also supports this conclusion that Au atoms preferably occupy the icosahedral core of $Au_xAg_{44-x}(SR)_{30}$, and that for x=12, the $Au_{12}Ag_{32}(SR)_{30}$ structure would be identical to that of the reported crystal structure of $Au_{12}Ag_{32}(SR)_{30}$ [Desireddy, A et al., *Nature* 2013, *501*, 399].

The present invention shows the energetics of Au-SH and Ag-SH fragments in the unalloyed clusters, and compared this with the energetics of single metal atom substitution to obtain further clues on the mechanism and its driving force. There are three possible Au-SR fragment positions in $Au_{25}(SR)_{18}$ and four different Ag-SR fragments in $Ag_{44}(SR)_{30}$, as shown in Figure 33. The reaction energies of Ag-SR/Au-SR substitution for both clusters are energetically favourable and exothermic (Table 6 & 8). This further supports the observation of M-SR exchange in mass spectrometric measurements. Thus, M-SR ex-change represents another pathway in the reaction mechanism and contributes to making the overall reaction exothermic. Furthermore, the presence of various possible substituent positions available in these clusters, especially in $Ag_{44}(SR)_{30}$ also suggest that entropic factors might also contribute to the lowering of the free energy of the reaction. In summary, calculations suggest that the driving force behind the inter-cluster M and M-SR exchanges is the lowering of the total energy of the reaction mainly by the formation of $Au_xAg_{44-x}(SR)_{30}$ clusters.

Table 1 Energies for the substitution reaction of (A) Au in $Ag_{44}(SR)_{30}$, (B) Ag in $Au_{25}(SR)_{18}$ and (C) the overall reaction energies (in eV) as a function of their positions in product clusters, $Au_xAg_{44-x}(SR)_{30}$ and $Au_{25-x}Ag_x(SR)_{18}$ for x=1. Locations of substitution for each cluster are described in the computational details.

(A)

Location of Au in $Au_xAg_{44-x}(SR)_{30}$	ΔE/eV
Icosahedron (I)	-0.72
Dodecahedron: cube vertex (D_{cv})	-0.14
Dodecahedron: cube face (D_{cf})	-0.32
Staples (S)	-0.48

(B)

Location of Ag in $Au_{25-x}Ag_x(SR)_{18}$	ΔE/eV
Central atom (C)	+0.71
Icosahedron (I)	+0.23
Staples (S)	+0.44

(C)

Location of Ag in $Au_{25-x}Ag_x(SR)_{18}$	Locations of Au in $Au_xAg_{44-x}(SR)_{30}$			
	I	D_{cv}	D_{cf}	S
C	-0.015	+0.564	+0.388	+0.226
I	-0.486	+0.093	-0.083	-0.245
S	-0.276	+0.303	+0.127	-0.035

The present invention suggest that the metal-thiolate interface plays a significant role in the mechanism of the reaction. In thiolate-protected molecular metal clusters, these interfaces often assume the form of metal-thiolate staple/mount motifs. Atoms in these motifs are considered to be in M^I oxidation state while those in the core are considered to be in M^0 oxidation state. Ag clusters and nanoparticles reduce Au^I or Au^I-SR thiolates [Krishnadas, K. R et al., *Eur. J. Inorg. Chem.* 2014, *5*, 908; Udayabhaskararao, T et al., *Angew. Chem. Int. Ed.* 2012, *51*, 2155] due to the higher reduction potential of Au^I. At the sub-nanometer scale, conversely, gold clusters can also reduce Ag^I ions and Ag^I-thiolates,[Choi, J.-P et al., *J. Phys. Chem. C* 2010, *114*, 15890; Wu, Z et al., *Angew. Chem. Int. Ed.* 2012, *51*, 2934; Wang, M. et al., *Chem. Asian J.* 2014, *9*, 1006] even though such reduction is not feasible for the bulk forms of these metals. Therefore, redox processes might also occur between the clusters since they are composed of silver and gold atoms in both the M^0 and M^I states. The relative energies of the HOMO (d derived) and LUMO (*sp* derived) states of the $Au_{25}(SR)_{18}$ and $Ag_{44}(SR)_{30}$ and their alloy isomers determine the feasibility of electron transfer from one cluster to another and which would behave like donor or acceptor. The HOMO level of $Ag_{44}(SR)_{30}$ is about 3.8 eV higher than the LUMO of $Au_{25}(SR)_{18}$ (Table 9 and 10). This indicates that an electron transfer into the

states above the LUMO of $Au_{25}(SR)_{18}$ followed by non-radiative relaxation into other levels of the cluster would release enough energy to overcome activation energy barriers and to break bonds, possibly in the staples and the core, leading to partial fragmentation. Although both the clusters are overall negatively charged, locally the electric field in the neighborhood of the ligands is both inhomogenous [Chen, X. et al., *Nat. Commun.*2015, 6, 8921] and screened by the solvent molecules. Metallophilic interactions between the Au(I) and Ag(I) centres,[Ni, W.-X. et al., *J. Am. Chem. Soc.*2014, *136*, 9532; Nardi, M. et al., *ACS Nano* 2014, *8*, 8505] (closed shell species) could also occur if their relative orientations permit closer approach within less than 3-4 A°. Attractive π-π stacking interactions between these aromatic ligands may also occur. These intercations are expected to bring clusters into proximity and to find their suitable orientation.

Table 2: Isomers of $Ag_{43}Au(SH)_{30}$ and their energies

Isomer	Au location	Energy E/eV	$E-E_0$/eV
I	Central icosahedron	-349.995	-0.72
D_{cv}	Dodecahedron (cube vertex)	-349.416	-0.14
D_{cf}	Dodecahedron(cube face)	-349.592	-0.32
S	Staple	-349.754	-0.48

Table 3: Isomers of Au24Ag(SH)18and their energies

Isomer	Ag location	Energy E/eV	$E-E_0$/eV
C	Centre of icosahedron	-219.576	+0.71
I	Icosahedron	-220.047	+0.23
S	Staple	-219.837	+0.44

Table 4: Energies of undoped clusters, metal atoms, and metal-ligand fragments

Structure	E_0/eV
$Ag_{44}(SH)_{30}$	-349.275
$Au_{25}(SH)_{18}$	-220.281
Ag	-0.1862
Au	-0.2035
AgSH(-)	-8.658
AuSH(-)	-8.902

Table 5: Energies of the reaction, $Au + Ag_{44}(SR)_{30} \rightarrow AuAg_{43}(SR)_{30} + Ag$

Isomer	Position of Au in $AuAg_{43}(SR)_{30}$	Energy E/eV
I	Inner icosahedron	-0.70
D_{cf}	Dodecahedron Cube face	-0.30
D_{cv}	Dodecahedron Cube vertex	-0.12
S	Staples	-0.46

Table 6: Energies of the reaction, $Au\text{-}SR + Ag_{44}(SR)_{30} \rightarrow AuAg_{43}(SR)_{30} + Ag\text{-}SR$

Position of Au-SR in $AuAg_{43}(SR)_{30}$	Energy E/eV
Dodecahedron Cube vertex (F3)	+0.10
Dodecahedron Cube face (F4)	-0.07
Staples (F1 and F2)	-0.24

Table 7: Energies of the reaction, $Ag + Au_{25}(SR)_{18} \rightarrow Au_{24}Ag(SR)_{18} + Au$

Isomer	Position of Ag in $Au_{24}Ag(SR)_{18}$	EnergyE/eV
C	Centre of icosahedron	+0.69
I	Icosahedron	+0.22
S	Staples	+0.43

Table 8: Energies of reaction, $Ag\text{-}SR + Au_{25}(SR)_{18} \rightarrow Au_{24}Ag(SR)_{18} + Au\text{-}SR$

Position of Ag-SR in $Au_{24}Ag(SR)_{18}$	EnergyE/eV
Icosahedron (F3)	-0.01
Staples (F1 and F2)	+0.2

Table 9: HOMO-LUMO energy difference of un-exchanged and alloy clusters

Cluster	Metal substituent position	HOMO/eV	LUMO/eV	HOMO-LUMO Gap/eV	Fermi Energy/eV
$Ag_{44}(SH)_{30}$	none	2.59	3.45	0.86	3.01
$Ag_{43}Au(SH)_{30}$	I	2.57	3.44	0.87	3.01
$Ag_{43}Au(SH)_{30}$	D_{cv}	2.61	3.43	0.82	3.02
$Ag_{43}Au(SH)_{30}$	D_{cf}	2.634	3.442	0.81	3.039
$Ag_{43}Au(SH)_{30}$	S	2.632	3.440	0.808	3.036
$Au_{25}(SH)_{18}$	none	-2.525	-1.238	1.287	-1.881
$Au_{24}Ag(SH)_{18}$	C	-2.485	-1.349	1.136	-1.917
$Au_{24}Ag(SH)_{18}$	I	-2.505	-1.222	1.283	-1.864
$Au_{24}Ag(SH)_{18}$	S	-2.557	-1.299	1.258	-1.928

Table 10: Energy difference (in eV) between the HOMO of $AuAg_{43}(SR)_{30}$ and LUMO of $Au_{24}Ag\ (SR)_{18}$ as a function of the substituent positions

Au Position in Ag_{44} / Ag Position in Au_{25}	I	D_{cv}	D_{cf}	S
C	3.919	3.959	3.983	3.981
I	**3.792**	3.832	3.856	**3.854**
S	**3.869**	3.909	3.933	3.931

The observed inter-cluster reactions might occur via the following three stages. In the first stage, destabilization of clusters can occur upon their closer approach facilitated by redox

processes and/or metallophilic/π-π interactions. These factors could weaken the M-S bonds in the staples and may result in fragmentation. However, the exact reason behind the destabilisation and fragmentation of the clusters are not clear in the present studies.

In the next stage, the unstabilized clusters might undergo fragmentation to form small M-SR, M-$(SR)_2$, $M_2(SR)_3$, etc. units or clusters with partially-opened staples or mounts followed by the nucleophilic attack of these fragments onto the staples of the cluster. Considering the polar nature of the M-S bonds in the staples due to greater electronegativity of the sulfur atom, these fragments become nucleophilic in nature. Anionic fragments such as $M(SR)_2$ and $M_2(SR)_3$ (where M=Au/Ag), etc, have been observed in mass spectrometry of $Au_{25}(SR)_{18}$ and $Ag_{44}(SR)_{30}$.[Angel, L. A. et al., *ACS Nano* 2010, *4*, 4691; Desireddy, A. et al., *Nature* 2013, *501*, 399; Harkness, K. M. et al., *Nanoscale*, 2012, *4*, 4269] Among these fragments, Au-$(SR)_2$ and the $Ag(SR)_2$ are the two most abundant species (Figure 36) and may be the most probable nucleophiles in the reaction. Similar mechanisms have been observed in ligand exchange reactions of monolayer protected clusters [Fernando, A. et al., *Phys. Chem. C* 2015, *119*, 20179] and metal exchange reactions of small metal-thiolate complexes.[Autissier, V.et al., *Inorg. Chem.*2008, *47*, 6393; Hagen, K. S. et al., *Inorg. Chem.*1982, *21*, 3928]. However, the mechanisms of metal exchange in monolayer protected clusters have not been investigated thoroughly.

The proposed mechanism for the reaction between $Au_{25}(SR)_{18}$ and $Ag(SR)_2$ fragment resulting in the exchange of Au atoms and various Au-SR fragments is depicted in Figure 37 and 38. However, in the case of $Ag_{44}(SR)_{30}$ these reactions could consist of several steps of bond-breaking events due to the more complicated bonding network of the $Ag_2(SR)_5$ mounts. This mechanism shows that even though the M-$(SR)_2$ unit is involved in the reaction, the net result is the inclusion of either M or M-SR groups depending on the specific reaction pathways. The exchange of the Ag-SR and Au-SR units between the clusters could be facile as they may be considered to be isolobal fragments. Exchange of similar metal-ligand isolobal units are also commonly encountered in coordination complexes.[Goldman, A. S. et al., *J. Am. Chem. Soc.*1986, *108*, 89; Hor, T. S. A. et al., *J. Coord. Chem.* 1989, *20*, 311]

In the final stage of the reaction, the open staples or the mounts of the clusters containing the substituent can rearrange, reconstructing the overall structural framewrok with substituted metal atoms or ligands resulting in the final products.

An intuitive and alternative way of visualizing the structural changes during the reactions can be inferred from the recent structural model [Natarajan, G. et al., *J. Phys. Chem. C* 2015 DOI: 10.1021/acs.jpcc.5b08193] showing that $Au_{25}(SR)_{18}$ can be viewed as three interlocked (Borromean) $Au_8(SR)_6$ rings around the central gold atom (Figure 34). These rings in the destabilized clusters may undergo opening, and once the staple chains or mounts are opened, they become more flexible and assume elongated conformations which gives the atoms of their free ends greater reach with which to interact with the corresponding open chains or mounts on the other cluster. A similar reorganization of the staples has been proposed (theoretically) earlier.[Liu, C. et al., *J. Am. Chem. Soc.*2013, *135*, 18067] The ends of the open chains or mounts can interact more easily exchanging the M and the M-SR units between them. The ring model of $Au_{25}(SR)_{18}$ also suggests that inclusion of Ag into the Au_{13} core is not as significantly hindered from the steric factors as might be expected when $Au_{25}(SR)_{18}$ is viewed as separate core covered by $Au_2(SR)_3$ staples. The opening and reorganization of the chains or mounts away from the core would make the core atoms more exposed, and facile for reaction. This may also be facilitated by structural rearrangements in the core and staples, or $Au_8(SR)_6$ rings as a whole due to rearrangements in the positions of the individual $Au_8(SR)_6$-rings. This model is presented here with the sole objective of presenting an explanation for the observed reactions. Similarly, the icosahedral Ag atoms in $Ag_{44}(SR)_{30}$ become more accessible when certain Ag-S bonds are broken (Figure 35). Thus the current mechanistic model implies that M and M-SR substitutions in the staples can originate from the reactions and rearrangements involving the metal-thiolate fragments and the open chains and mounts, while substitutions of the core atoms could involve the exposed core of one of the clusters and the fragments or open chains or mounts of the other cluster.

The initially-formed alloy clusters with fewer numbers of substituents could also undergo similar reactions producing clusters with higher number of substituents until the thermodynamic equilibrium for the particular reactant concentration is reached (Figure 9-10). Final positions of the substituent metal atoms in the alloy clusters are dictated by their relative energies which depend on the number of the substituents and their positions, as mentioned earlier.

It may be appreciated by those skilled in the art that the drawings, examples and detailed description herein are to be regarded in an illustrative rather than a restrictive manner.

We Claim: **CLEAN COPY**

1. A method of making an noble metal alloy cluster of atomically precise composition by reacting two or more atomically precise monolayer protected noble metal clusters in solution, the said noble metal clusters includes metal-thiolate clusters, $Au_{25}(SR)_{18}$ and $Ag_{44}(SR)_{30}$, where SR represents an alkyl/aryl thiolate ligand which protect Au_{25} and Ag_{44} clusters; wherein the metal clusters undergo spontaneous inter-cluster reactions in solution at ambient conditions to form alloy clusters through exchange of metal atoms, protecting ligands and metal-thiolate fragments derived from the clusters.
2. The method as claimed in claim 1, wherein the ligand includes 2-phenylethanethiol (PET), n-butanethiol (n-BuSH), 4-fluorothiophenol (FTP).
3. The method as claimed in claim 1, wherein the metal clusters undergo spontaneous reaction in solution at ambient conditions in solvents including hydrocarbons, alcohols, ethers, halocarbons, esters, ketones, aldehydes, nitriles, amines, furans, carbon disulphide, or their mixtures.
4. The method as claimed in claim 1, wherein the inter-cluster alloying for heteroatom doping allows doping up to 20 Ag atoms into $Au_{25}(SR)_{18}$.
5. The method as claimed in claim 1, wherein the inter-cluster reactions occurs between metal clusters for making an alloy having the formula $Au_{25-x}Ag_x(PET)_{18-y}(FTP)_y$, wherein x,y represents (x=0,1-20; y=0,1-11).
6. The method as claimed in claim 1, wherein the reactions occur between clusters having same and/or different ligands.
7. The method as claimed in claim 1, wherein density functional theory (DFT) is used to calculate energies of the reactants [$Au_{25}(SR)_{18}$ and $Ag_{44}(SR)_{30}$], the products [$Au_{25-x}Ag_x(SR)_{18}$ and $Au_xAg_{44-x}(SR)_{30}$] and the likely species being exchanged in the intermediate steps such as metal atoms (M), and thiolate fragments (M-SR).
8. The method as claimed in claim 1, wherein the DFT calculations show that in case of $Au_xAg_{44-x}(SR)_{30}$, Au atoms prefer to occupy the icosahedral core followed by the outer staples and lastly the inner dodecahedron.
9. The method as claimed in claim 1, wherein the overall reaction is energetically favorable due to the lowering of the energy of Au or Au-SR substitution into $Ag_{44}(SR)_{30}$ rather than the Ag or Ag-SR substitution into $Au_{25}(SR)_{18}$.
10. The method as claimed in claim 1, wherein making water soluble alloys of precise composition with enhanced visible luminescence is suitable for chemical or biological applications.

11. The method as claimed in claim 1, wherein making alloy clusters by reactions between atomically precise clusters or nanoparticles from Au and Ag including Au_{38}, Au_{102}, Ag_{25} and Ag_{152} with ligands including phenylethanethiol, fluorothiophenol and mercaptobenzoic acid.
12. The method as claimed in claim 1, wherein the alloy clusters of precise composition by inter cluster reactions exhibits properties including luminescence, catalysis, magnetism, sensing, data storage, electrical conductivity.

Dated at Chennai this November 20, 2019

Signature: 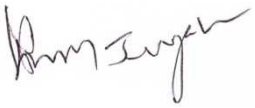

D. Moses Jeyakaran
Advocate & Patent Agent
IN/PA — 369

METHOD OF MAKING ALLOYS OF PRECISE COMPOSITION USING INTER-CLUSTER REACTIONS IN SOLUTION

ABSTRACT

The present invention relates to a method of making a noble metal alloy cluster by solution state reactions of atomically precise nanoclusters. The invention performs inter-cluster reactions between atomically precise, monolayer protected noble metal clusters using $Au_{25}(SR)_{18}$ and $Ag_{44}(SR)_{30}$ (RS-= alkyl/aryl thiolate) as model compounds. Mass spectrometric measurements both by electrospray ionization and matrix assisted laser desorption ionization show that the reaction occurs through the exchange of metal atoms and protecting ligands of the clusters. Inter-cluster alloying is a facile method for heteroatom doping into $Au_{25}(SR)_{18}$, as observed by doping up to twenty Ag atoms. Metal core-thiolate interfaces in these clusters play a crucial role in inducing these reactions and also affect rates of these reactions. Such reactions provide a unique way of tuning properties of nanoscale particles of precise composition.

METHOD OF MAKING ALLOYS OF PRECISE COMPOSITION USING INTER-CLUSTER REACTIONS IN SOLUTION

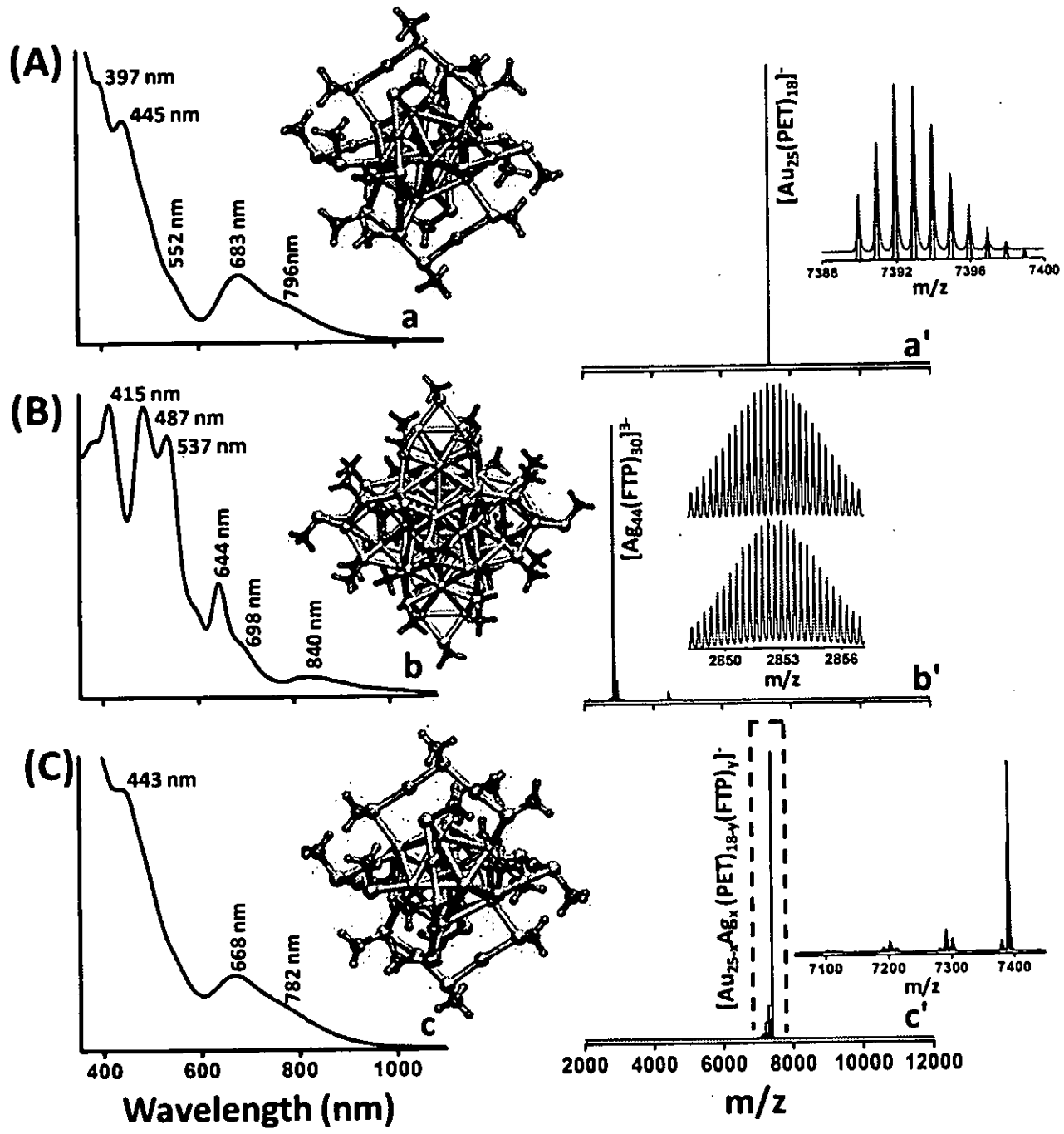

FIGURE 1

Signature:

D. Moses Jeyakaran
Advocate & Patent Agent
IN/PA — 369

METHOD OF MAKING ALLOYS OF PRECISE COMPOSITION USING INTER-CLUSTER REACTIONS IN SOLUTION

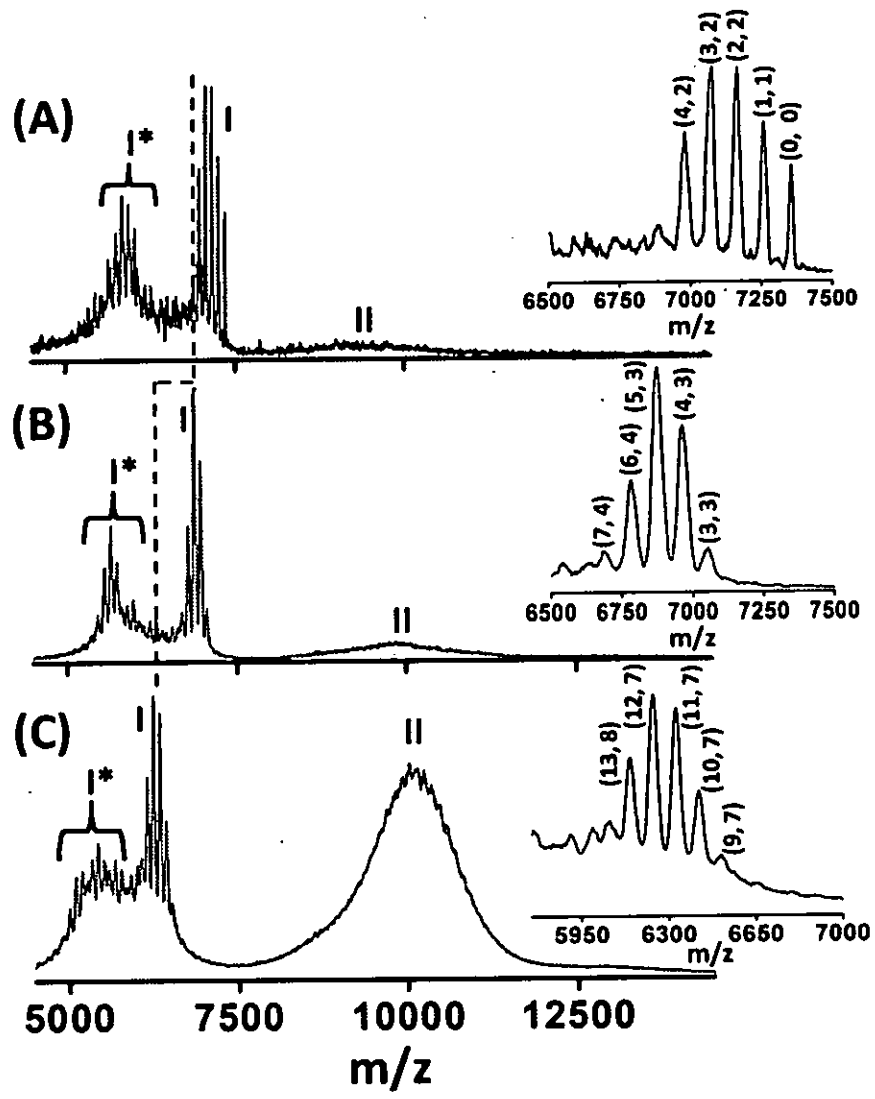

FIGURE 2

Signature:

D. Moses Jeyakaran
Advocate & Patent Agent
IN/PA — 369

METHOD OF MAKING ALLOYS OF PRECISE COMPOSITION USING INTER-CLUSTER REACTIONS IN SOLUTION

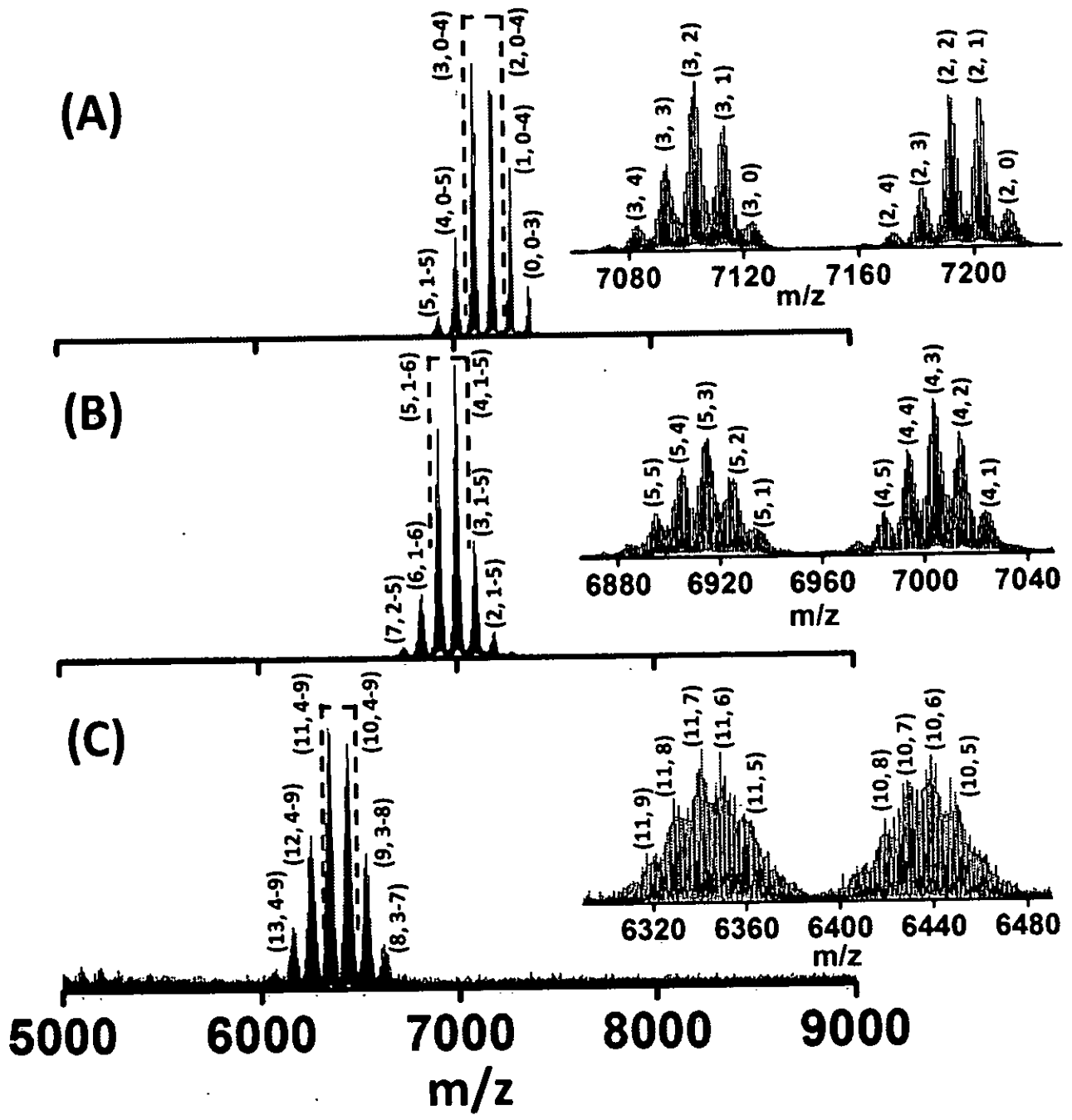

FIGURE 3

Signature:

D. Moses Jeyakaran
Advocate & Patent Agent
IN/PA — 369

32

METHOD OF MAKING ALLOYS OF PRECISE COMPOSITION USING INTER-CLUSTER REACTIONS IN SOLUTION

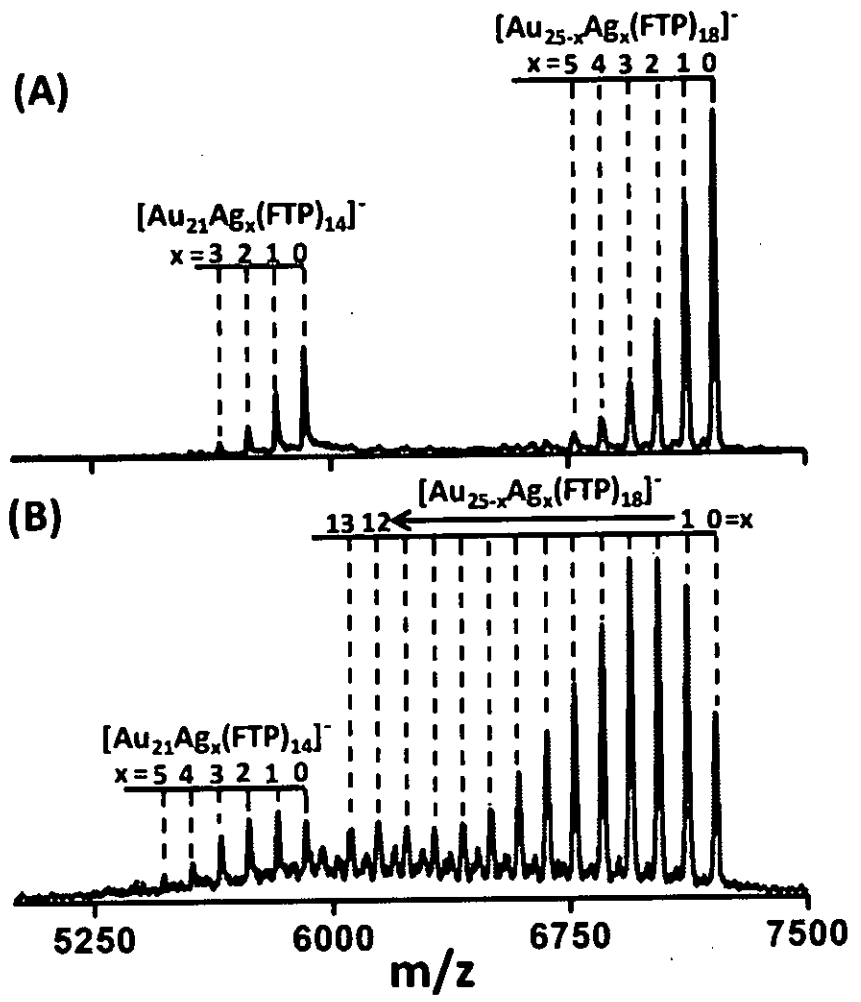

FIGURE 4

Signature:

D. Moses Jeyakaran
Advocate & Patent Agent
IN/PA — 369

METHOD OF MAKING ALLOYS OF PRECISE COMPOSITION USING INTER-CLUSTER REACTIONS IN SOLUTION

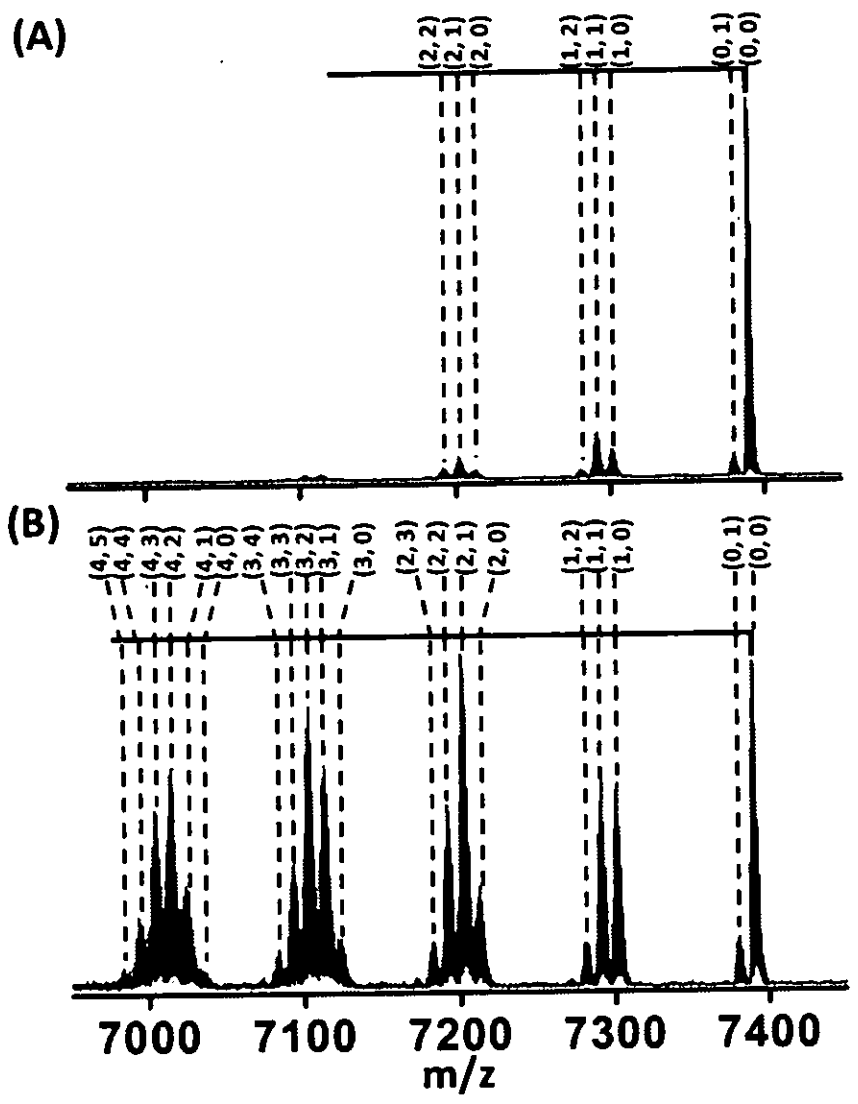

FIGURE 5

Signature:

D. Moses Jeyakaran
Advocate & Patent Agent
IN/PA — 369

METHOD OF MAKING ALLOYS OF PRECISE COMPOSITION USING INTER-CLUSTER REACTIONS IN SOLUTION

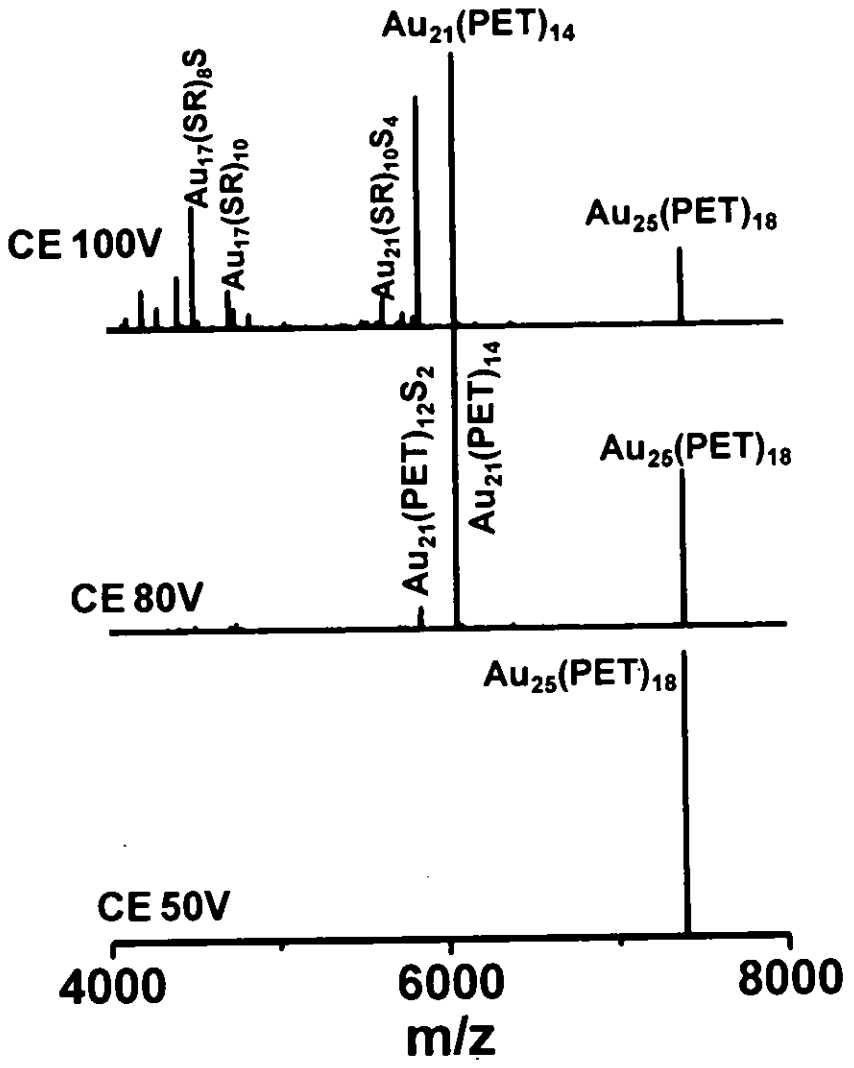

FIGURE 6

Signature:

D. Moses Jeyakaran
Advocate & Patent Agent
IN/PA — 369

METHOD OF MAKING ALLOYS OF PRECISE COMPOSITION USING INTER-CLUSTER REACTIONS IN SOLUTION

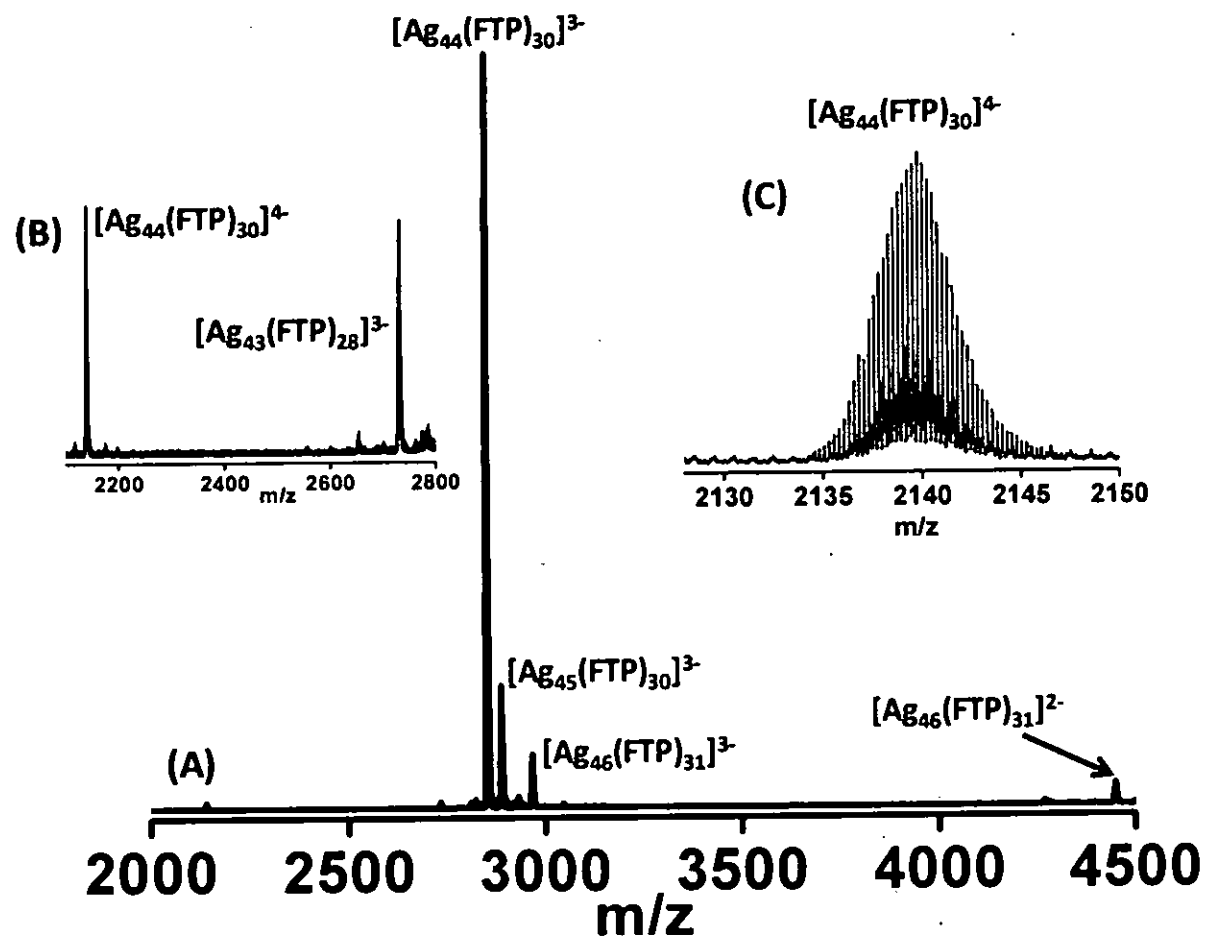

FIGURE 7

Signature:

D. Moses Jeyakaran
Advocate & Patent Agent
IN/PA — 369

METHOD OF MAKING ALLOYS OF PRECISE COMPOSITION USING INTER-CLUSTER REACTIONS IN SOLUTION

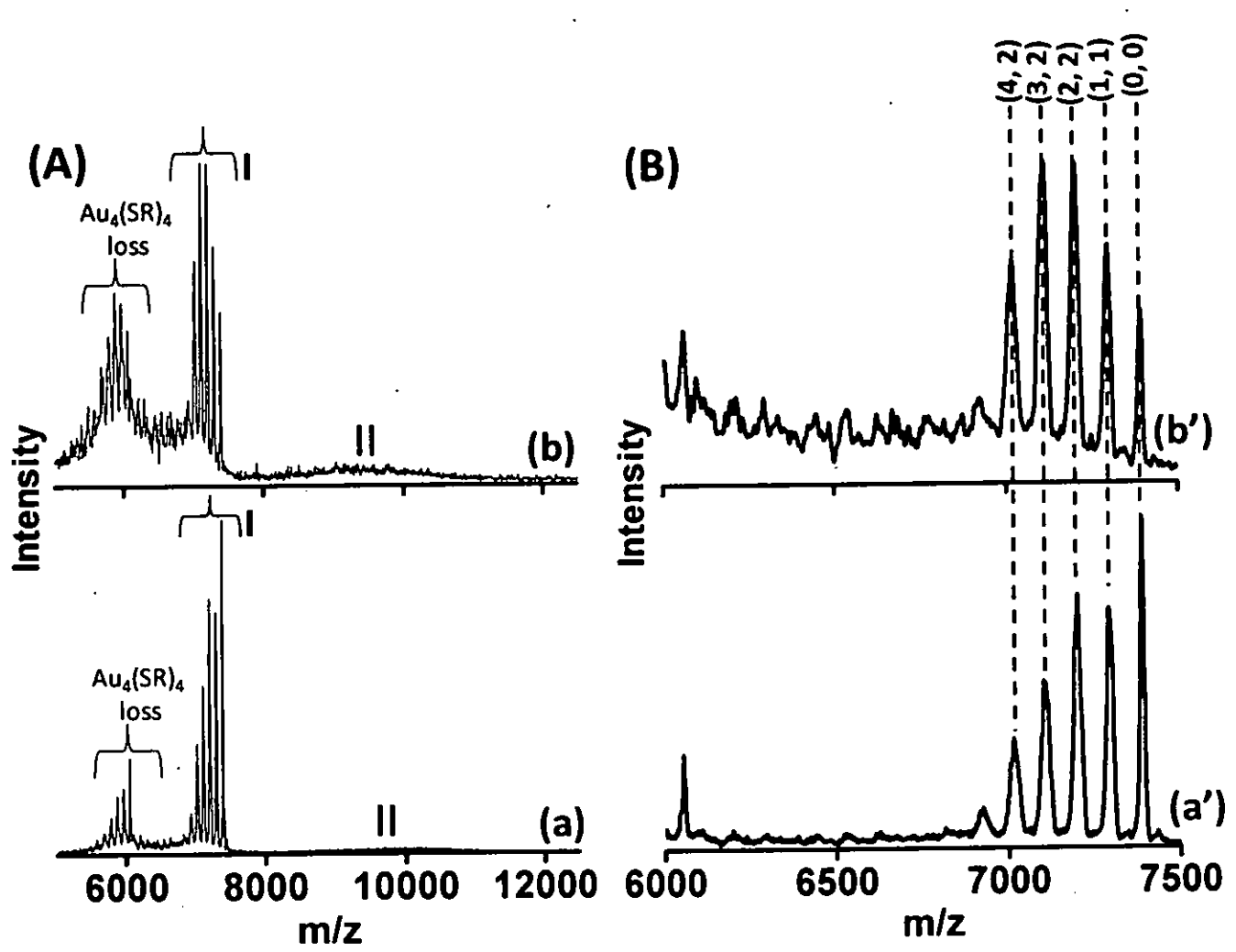

FIGURE 8

Signature:

D. Moses Jeyakaran
Advocate & Patent Agent
IN/PA — 369

METHOD OF MAKING ALLOYS OF PRECISE COMPOSITION USING INTER-CLUSTER REACTIONS IN SOLUTION

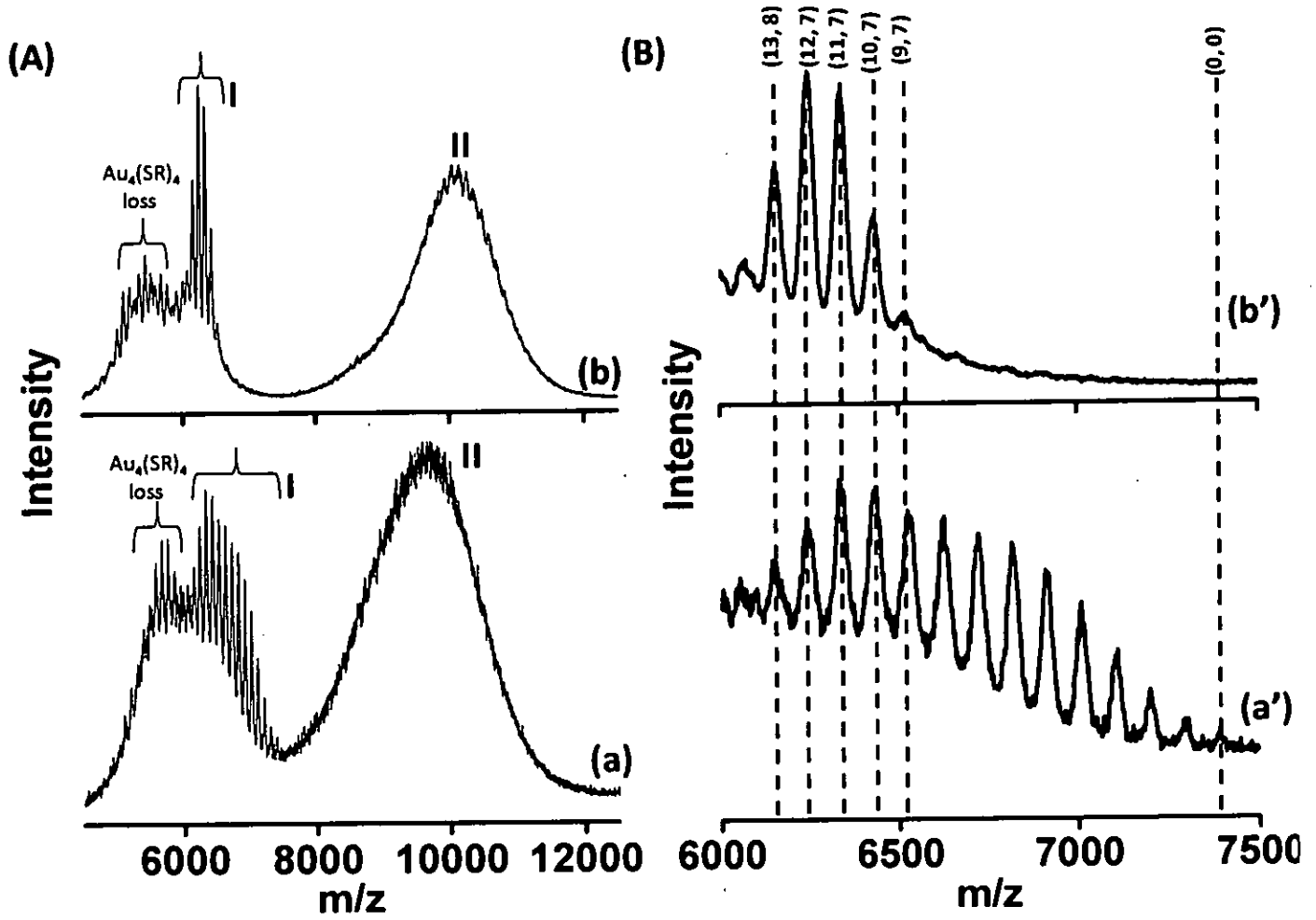

FIGURE 9

Signature:

D. Moses Jeyakaran
Advocate & Patent Agent
IN/PA — 369

METHOD OF MAKING ALLOYS OF PRECISE COMPOSITION USING INTER-CLUSTER REACTIONS IN SOLUTION

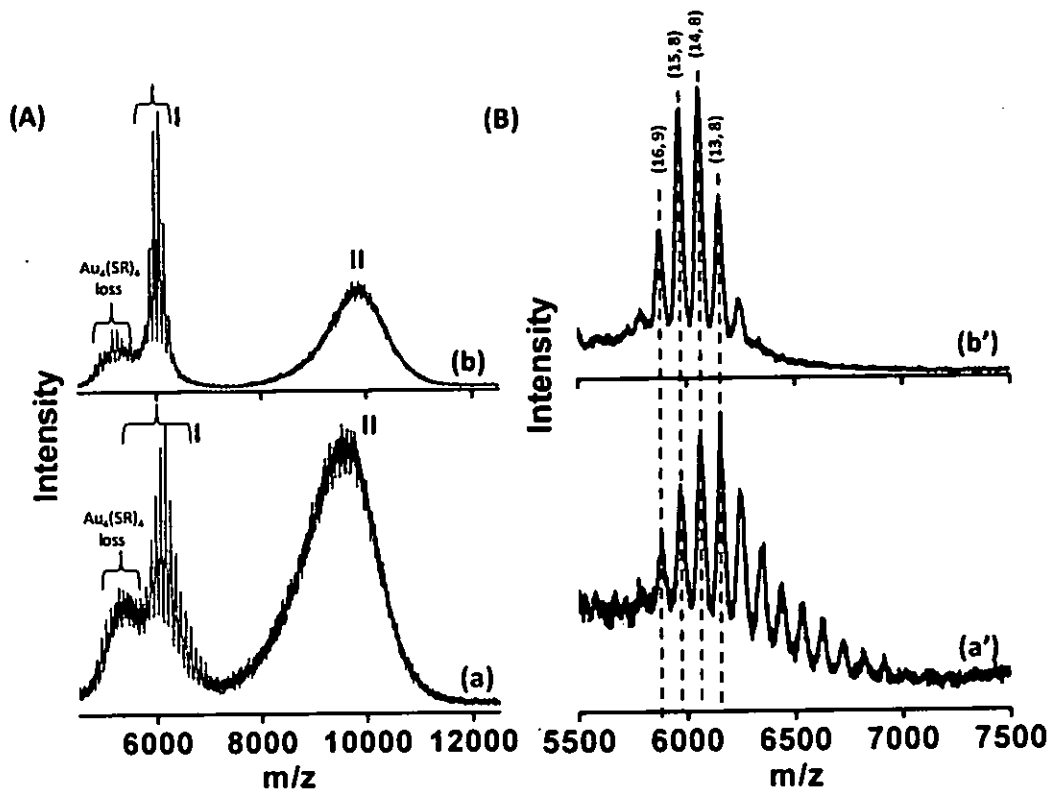

FIGURE 10

Signature:

D. Moses Jeyakaran
Advocate & Patent Agent
IN/PA — 369

METHOD OF MAKING ALLOYS OF PRECISE COMPOSITION USING INTER-CLUSTER REACTIONS IN SOLUTION

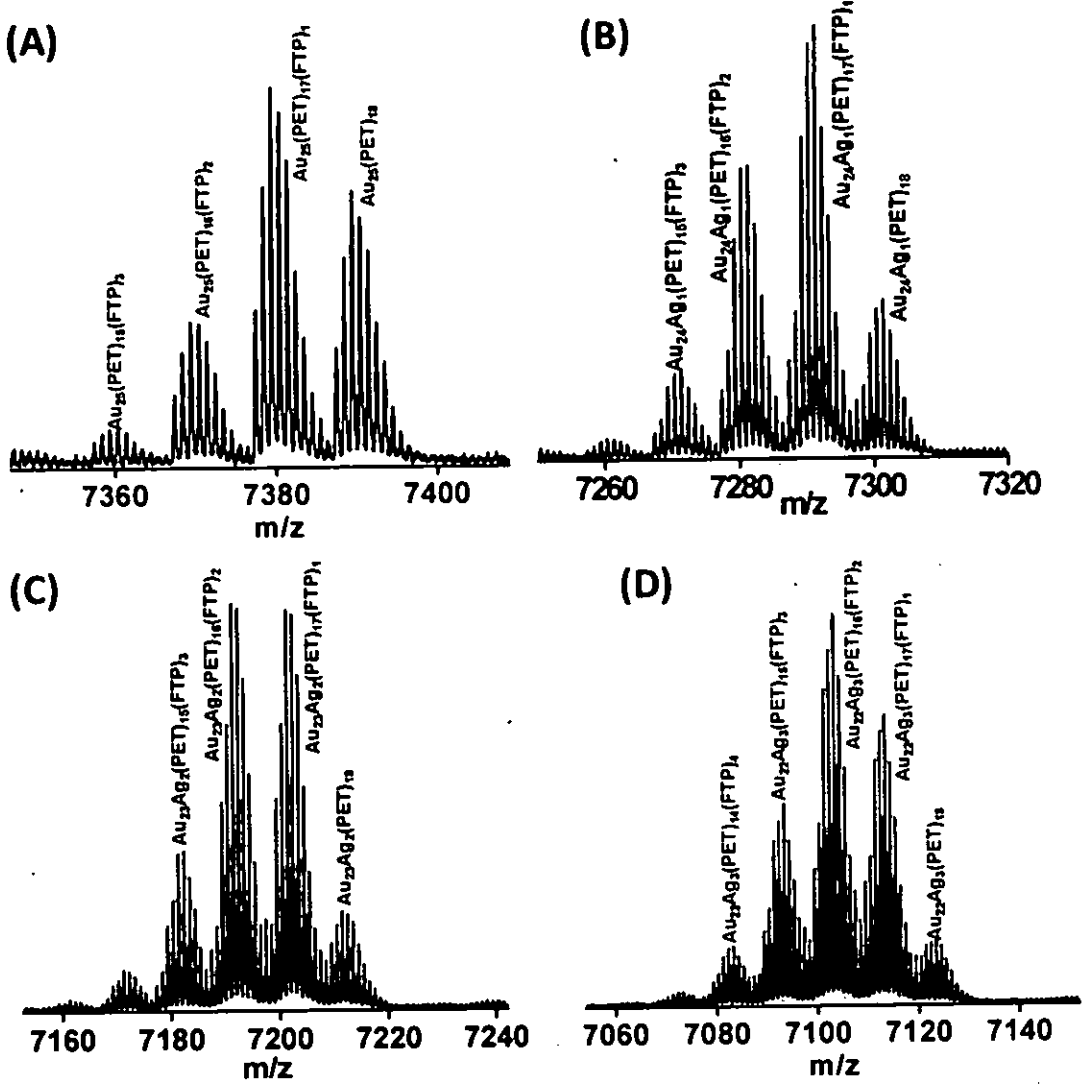

FIGURE 11

Signature:

D. Moses Jeyakaran
Advocate & Patent Agent
IN/PA — 369

METHOD OF MAKING ALLOYS OF PRECISE COMPOSITION USING INTER-CLUSTER REACTIONS IN SOLUTION

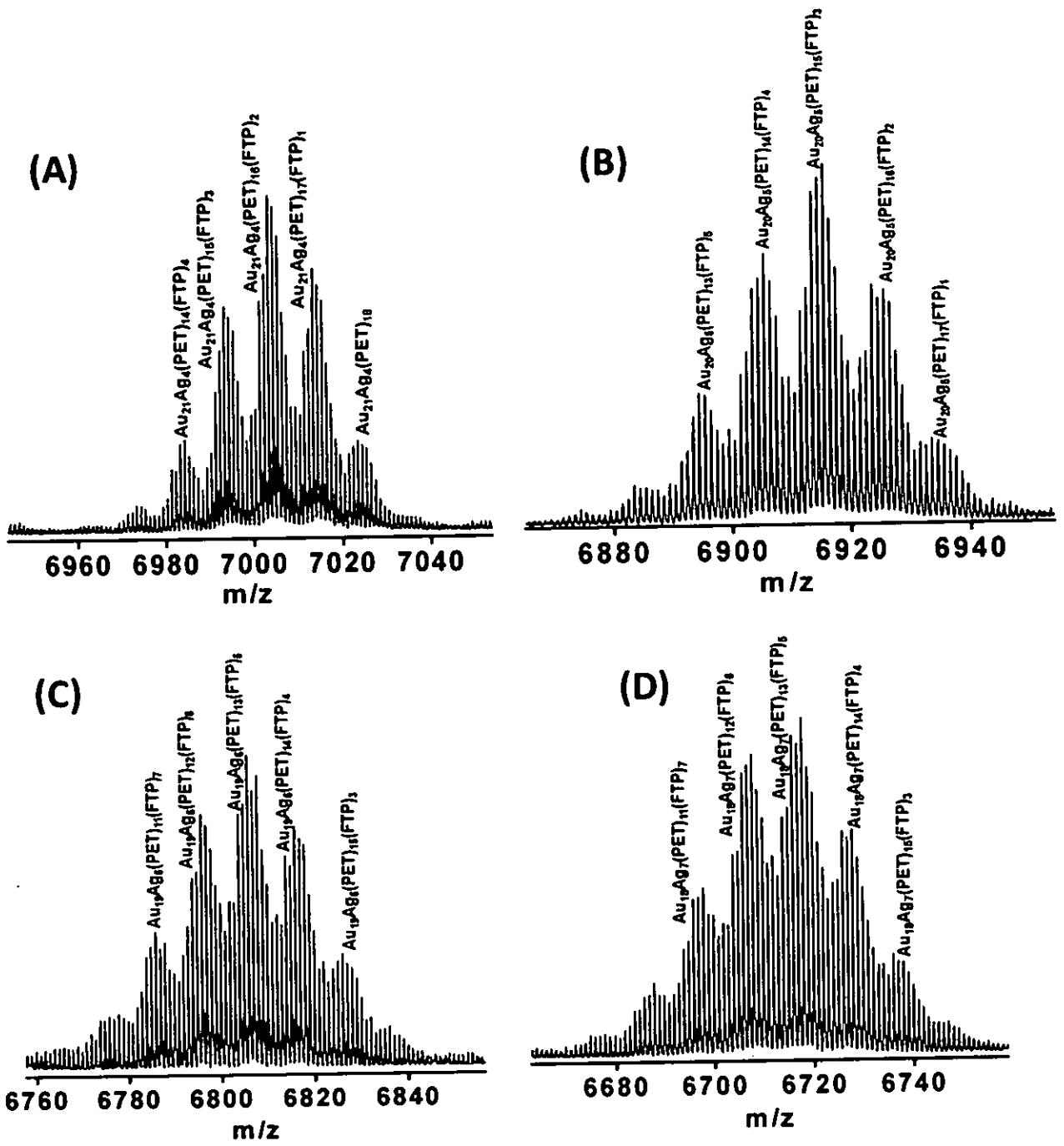

FIGURE 12

Signature:

D. Moses Jeyakaran
Advocate & Patent Agent
IN/PA — 369

METHOD OF MAKING ALLOYS OF PRECISE COMPOSITION USING INTER-CLUSTER REACTIONS IN SOLUTION

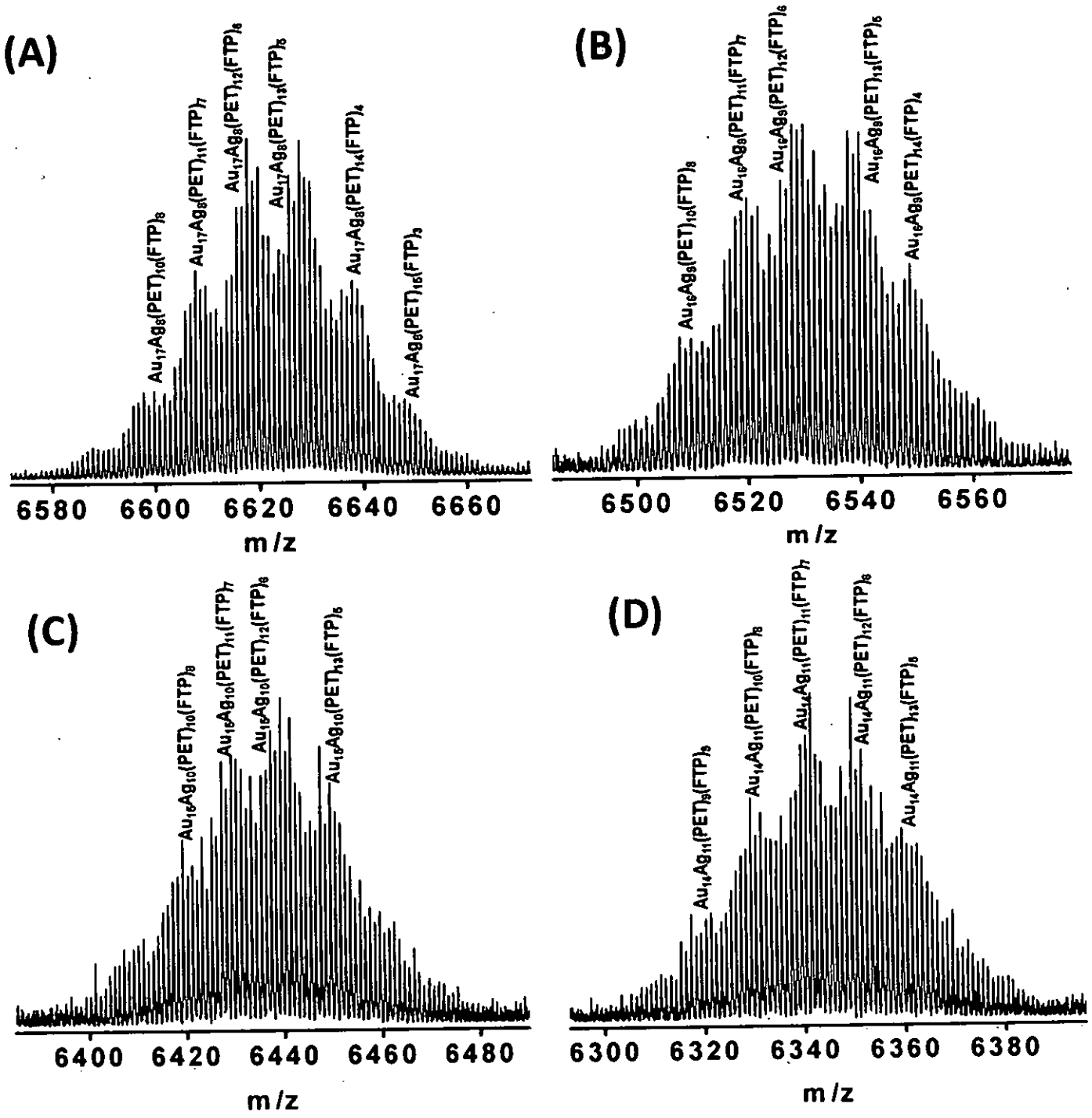

FIGURE 13

Signature:

D. Moses Jeyakaran
Advocate & Patent Agent
IN/PA — 369

METHOD OF MAKING ALLOYS OF PRECISE COMPOSITION USING INTER-CLUSTER REACTIONS IN SOLUTION

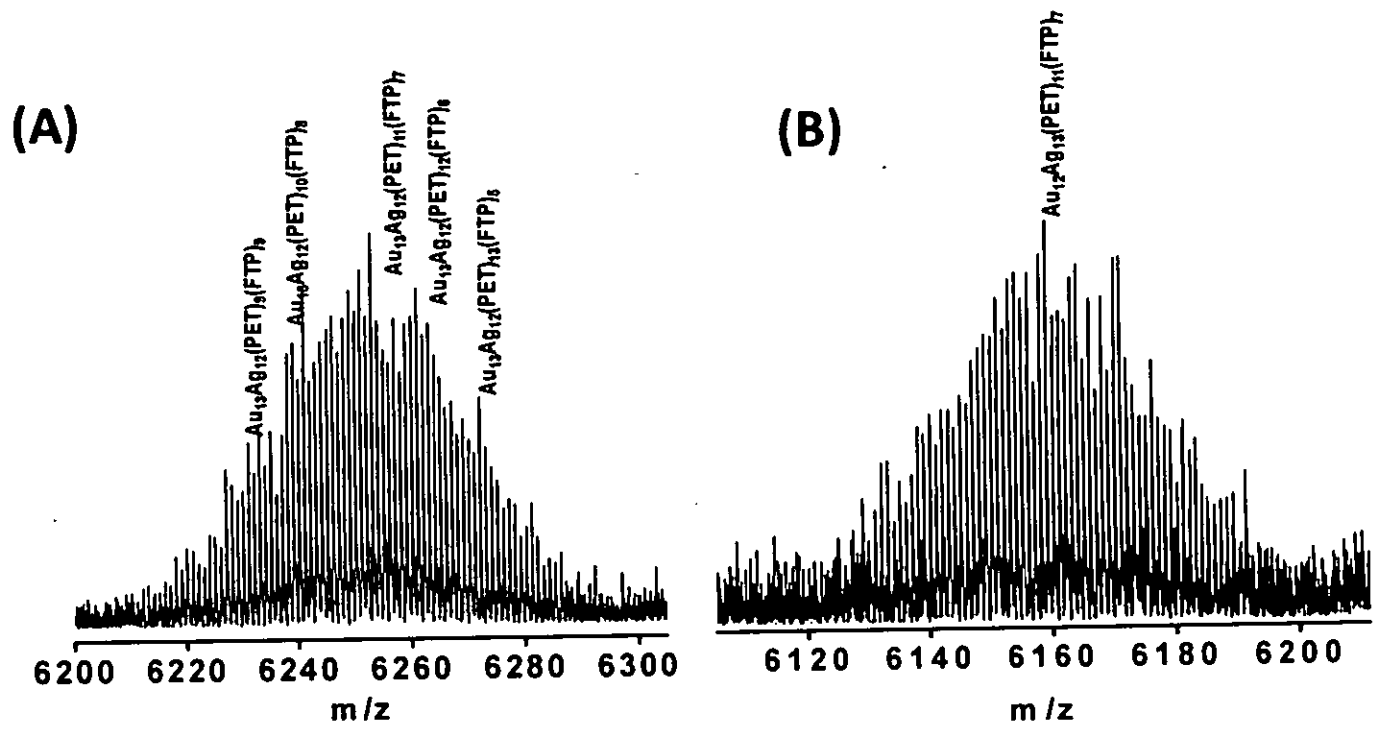

FIGURE 14

Signature:

D. Moses Jeyakaran
Advocate & Patent Agent
IN/PA — 369

METHOD OF MAKING ALLOYS OF PRECISE COMPOSITION USING INTER-CLUSTER REACTIONS IN SOLUTION

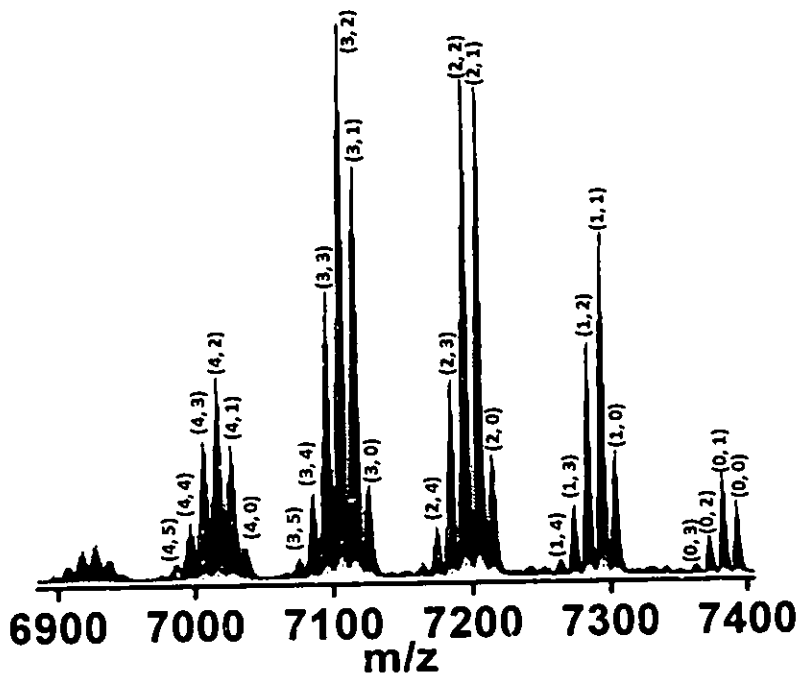

FIGURE 15

Signature:

D. Moses Jeyakaran
Advocate & Patent Agent
IN/PA — 369

METHOD OF MAKING ALLOYS OF PRECISE COMPOSITION USING INTER-CLUSTER REACTIONS IN SOLUTION

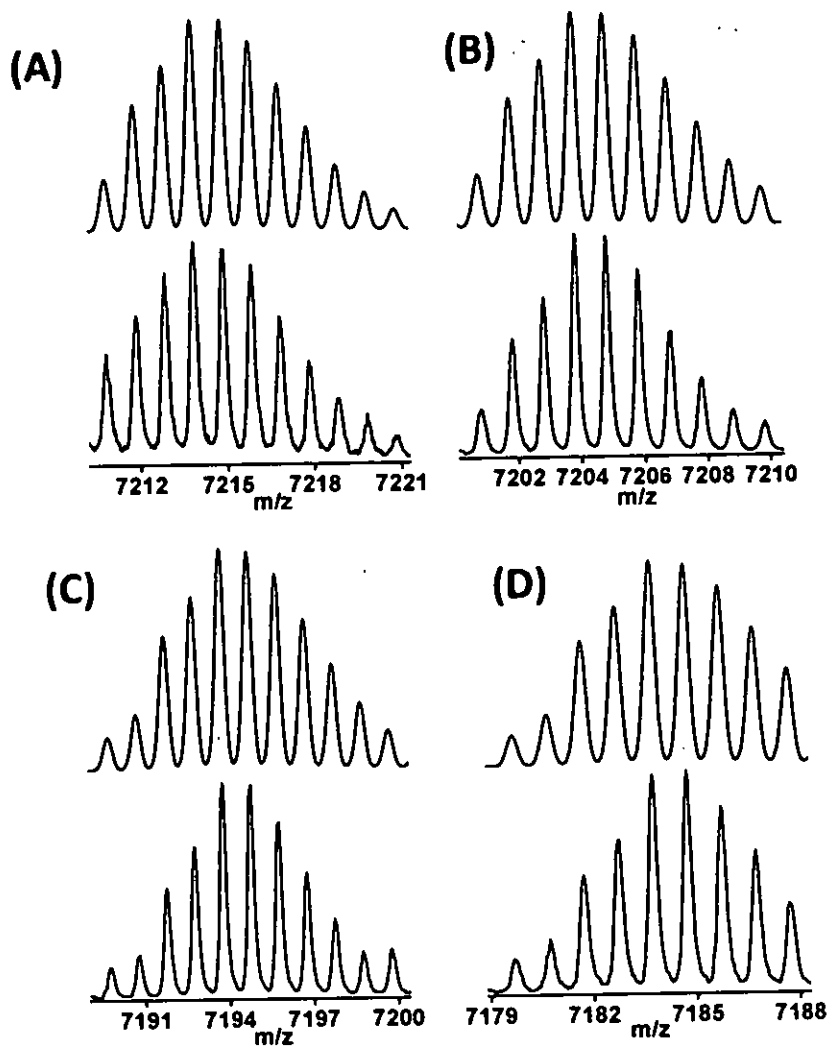

FIGURE 16

Signature:

D. Moses Jeyakaran
Advocate & Patent Agent
IN/PA — 369

INDIAN INSTITUTE OF TECHNOLOGY MADRAS

METHOD OF MAKING ALLOYS OF PRECISE COMPOSITION USING INTER-CLUSTER REACTIONS IN SOLUTION

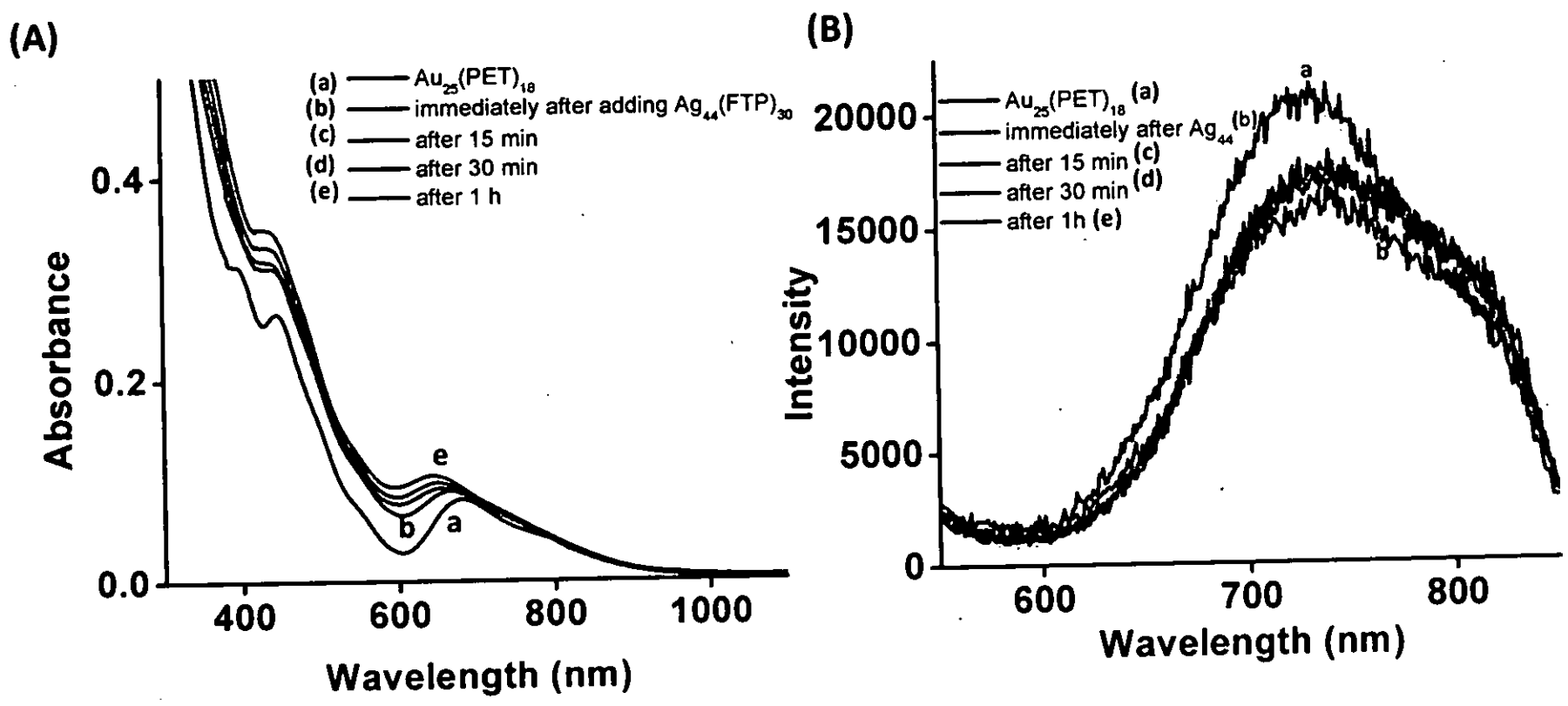

FIGURE 17

Signature:

D. Moses Jeyakaran
Advocate & Patent Agent
IN/PA — 369

METHOD OF MAKING ALLOYS OF PRECISE COMPOSITION USING INTER-CLUSTER REACTIONS IN SOLUTION

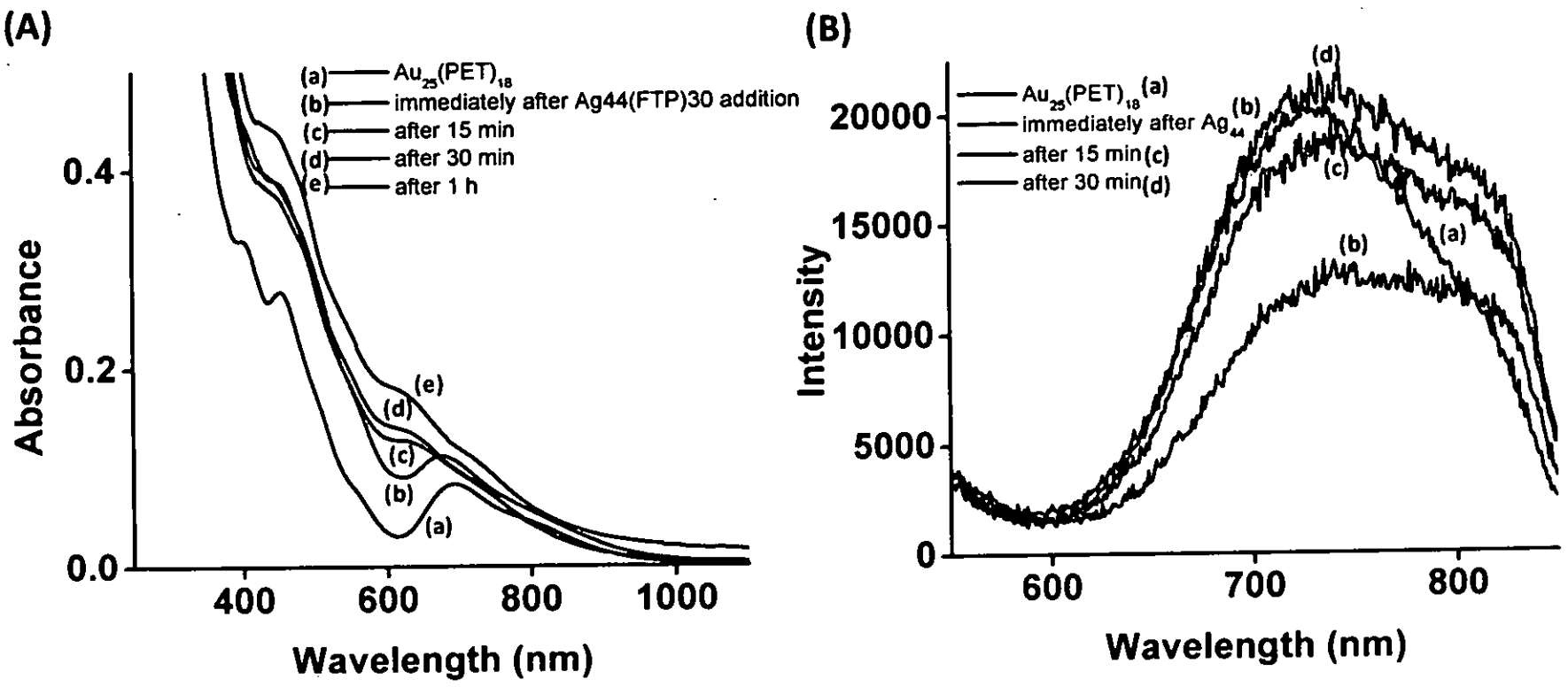

FIGURE 18

Signature:

D. Moses Jeyakaran
Advocate & Patent Agent
IN/PA — 369

METHOD OF MAKING ALLOYS OF PRECISE COMPOSITION USING INTER-CLUSTER REACTIONS IN SOLUTION

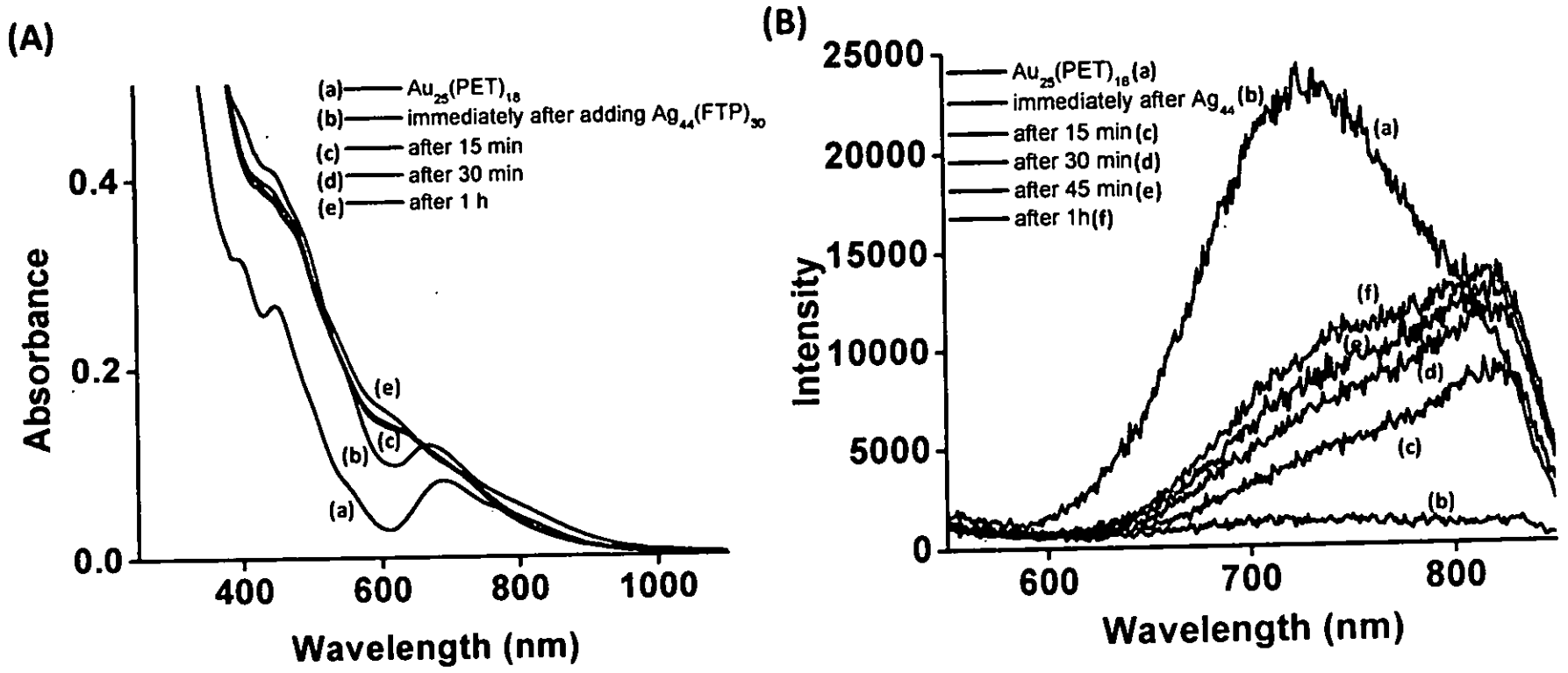

FIGURE 19

Signature:

D. Moses Jeyakaran
Advocate & Patent Agent
IN/PA — 369

METHOD OF MAKING ALLOYS OF PRECISE COMPOSITION USING INTER-CLUSTER REACTIONS IN SOLUTION

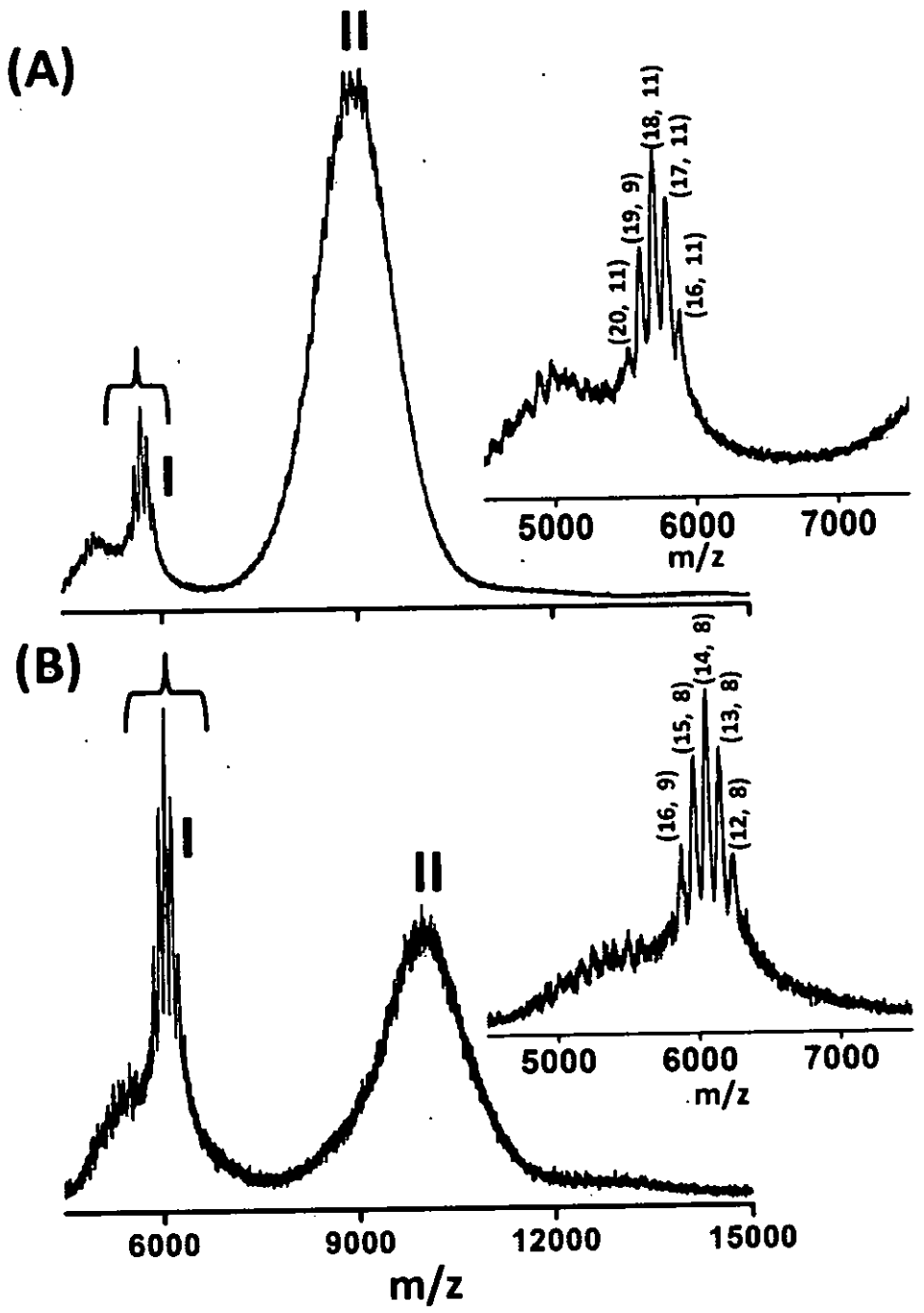

FIGURE 20

Signature:

D. Moses Jeyakaran
Advocate & Patent Agent
IN/PA — 369

METHOD OF MAKING ALLOYS OF PRECISE COMPOSITION USING INTER-CLUSTER REACTIONS IN SOLUTION

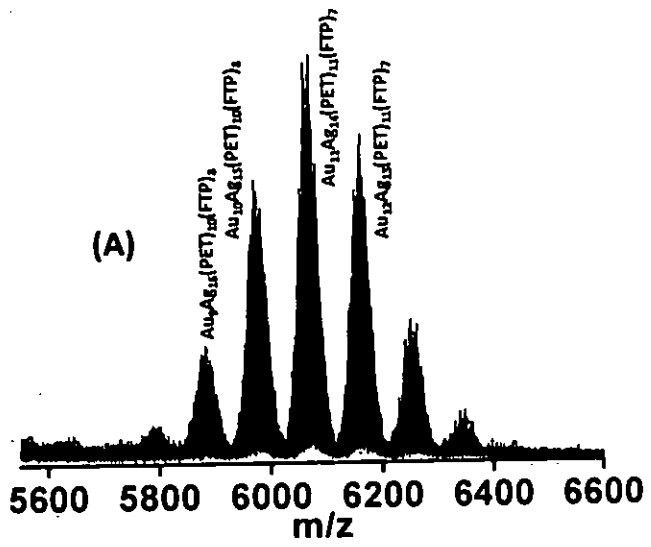

FIGURE 21

Signature:

D. Moses Jeyakaran
Advocate & Patent Agent
IN/PA — 369

METHOD OF MAKING ALLOYS OF PRECISE COMPOSITION USING INTER-CLUSTER REACTIONS IN SOLUTION

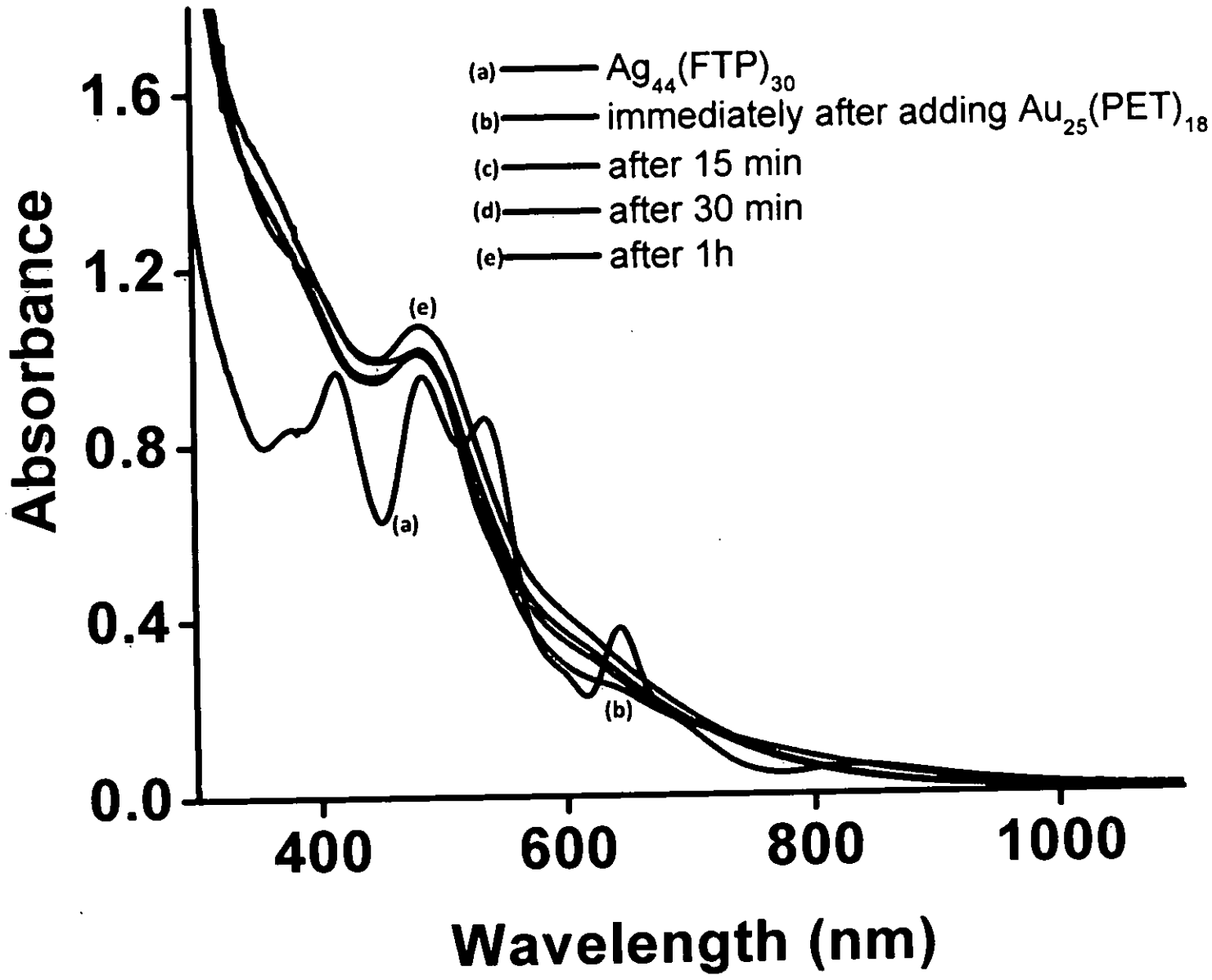

FIGURE 22

Signature:

D. Moses Jeyakaran
Advocate & Patent Agent
IN/PA — 369

METHOD OF MAKING ALLOYS OF PRECISE COMPOSITION USING INTER-CLUSTER REACTIONS IN SOLUTION

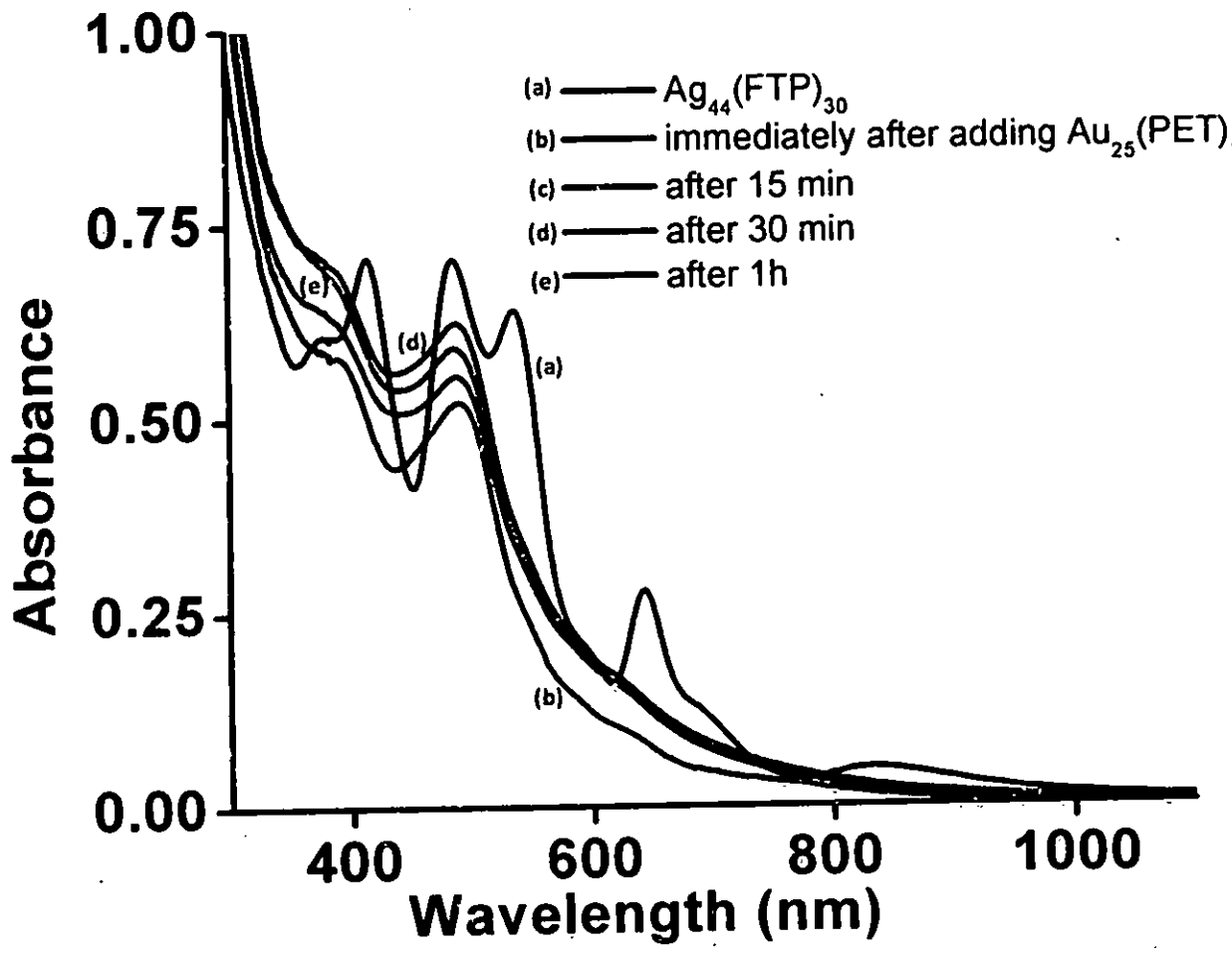

FIGURE 23

Signature:

D. Moses Jeyakaran
Advocate & Patent Agent
IN/PA — 369

METHOD OF MAKING ALLOYS OF PRECISE COMPOSITION USING INTER-CLUSTER REACTIONS IN SOLUTION

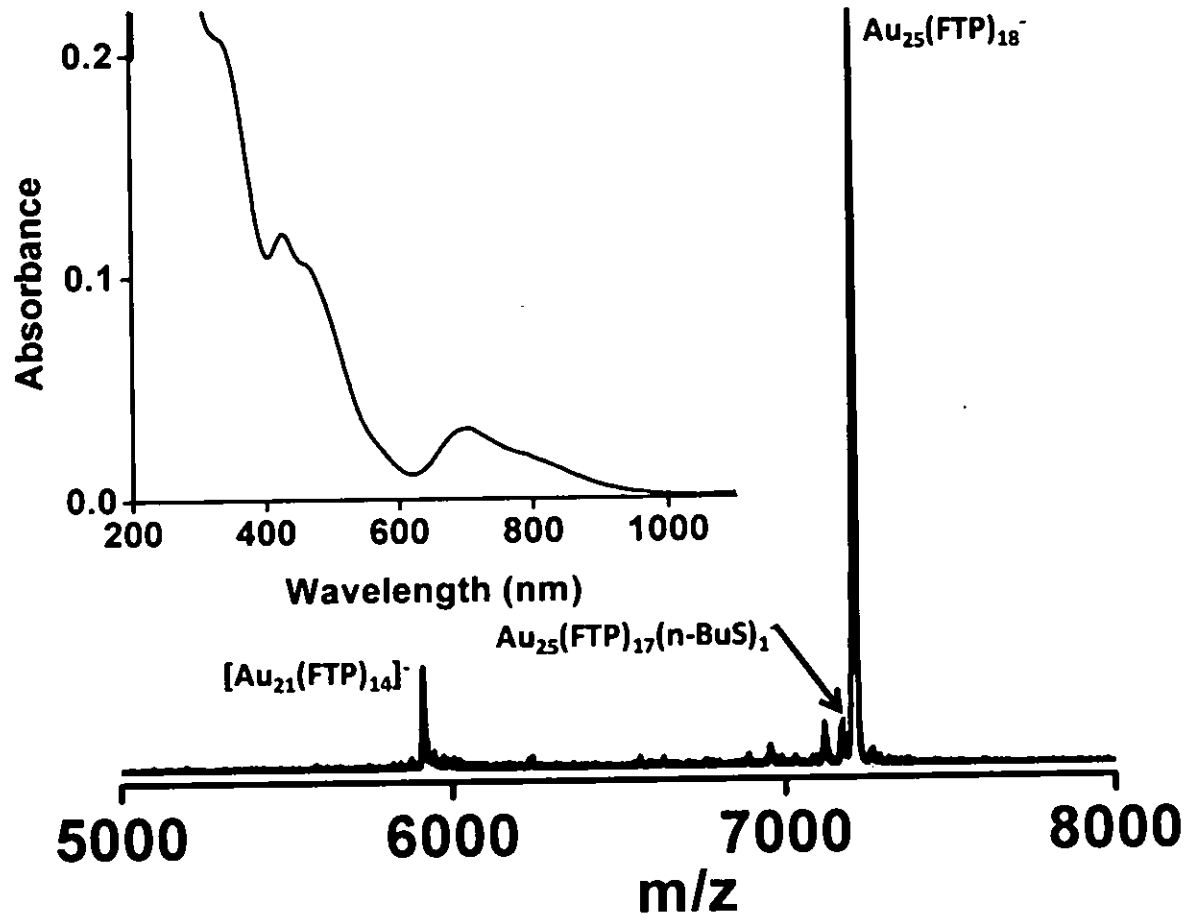

FIGURE 24

Signature:

D. Moses Jeyakaran
Advocate & Patent Agent
IN/PA — 369

METHOD OF MAKING ALLOYS OF PRECISE COMPOSITION USING INTER-CLUSTER REACTIONS IN SOLUTION

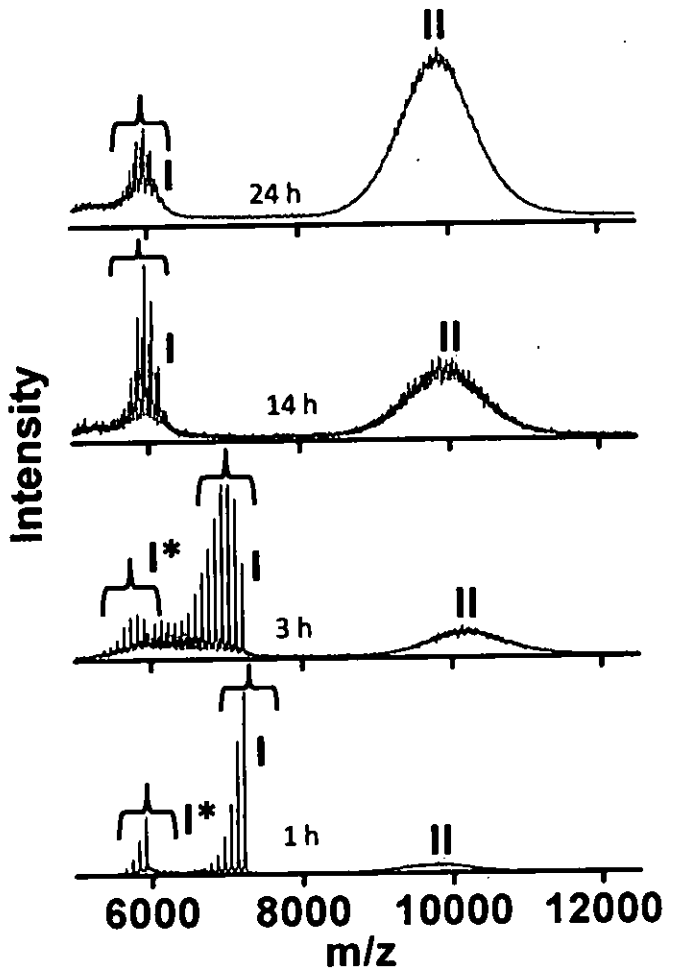

FIGURE 25

Signature:

D. Moses Jeyakaran
Advocate & Patent Agent
IN/PA — 369

METHOD OF MAKING ALLOYS OF PRECISE COMPOSITION USING INTER-CLUSTER REACTIONS IN SOLUTION

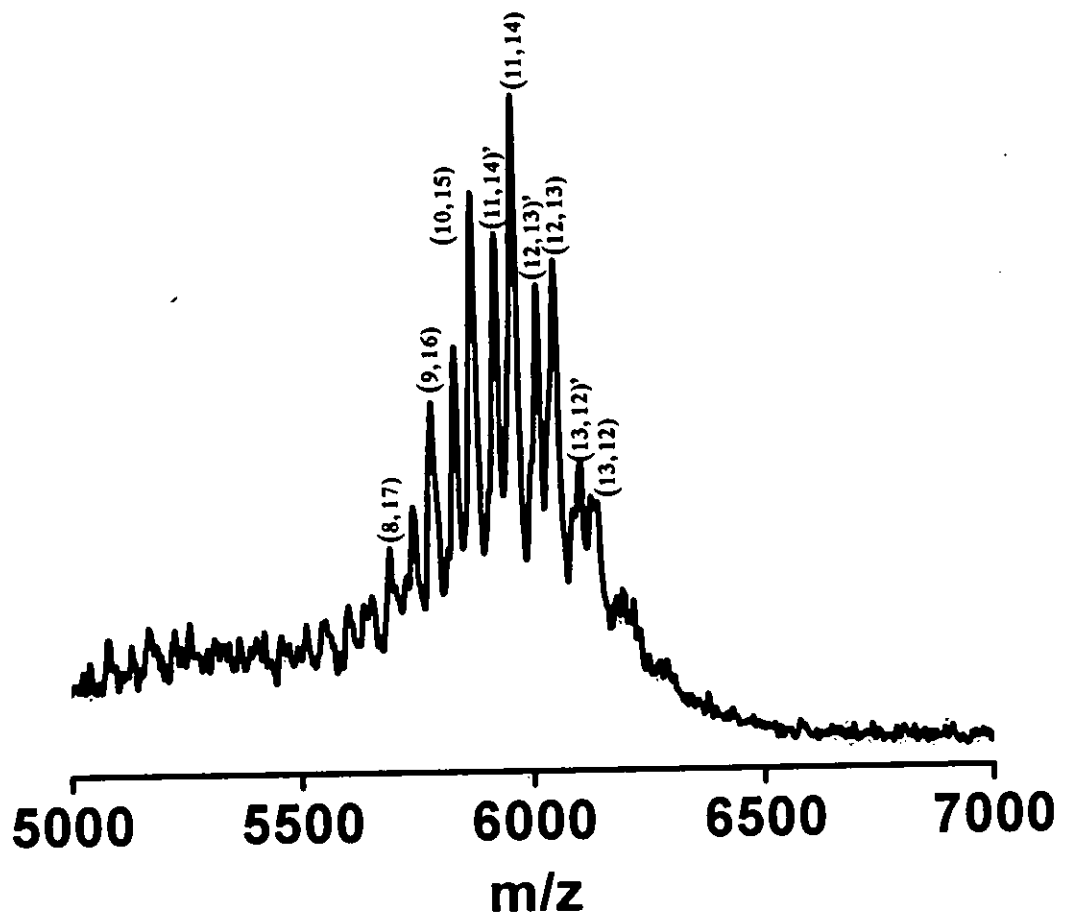

FIGURE 26

Signature:

D. Moses Jeyakaran
Advocate & Patent Agent
IN/PA — 369

METHOD OF MAKING ALLOYS OF PRECISE COMPOSITION USING INTER-CLUSTER REACTIONS IN SOLUTION

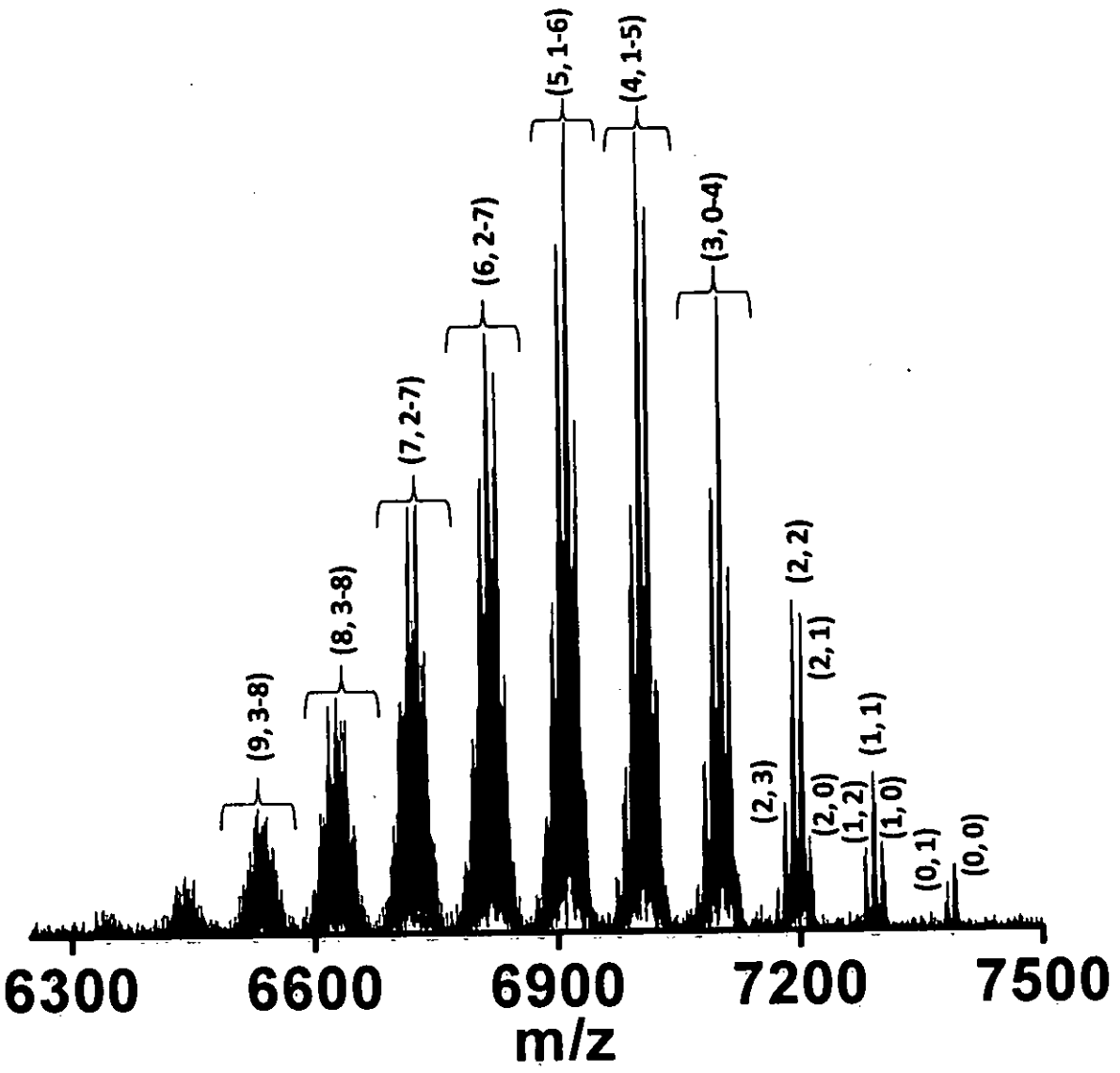

FIGURE 27

Signature:

D. Moses Jeyakaran
Advocate & Patent Agent
IN/PA — 369

METHOD OF MAKING ALLOYS OF PRECISE COMPOSITION USING INTER-CLUSTER REACTIONS IN SOLUTION

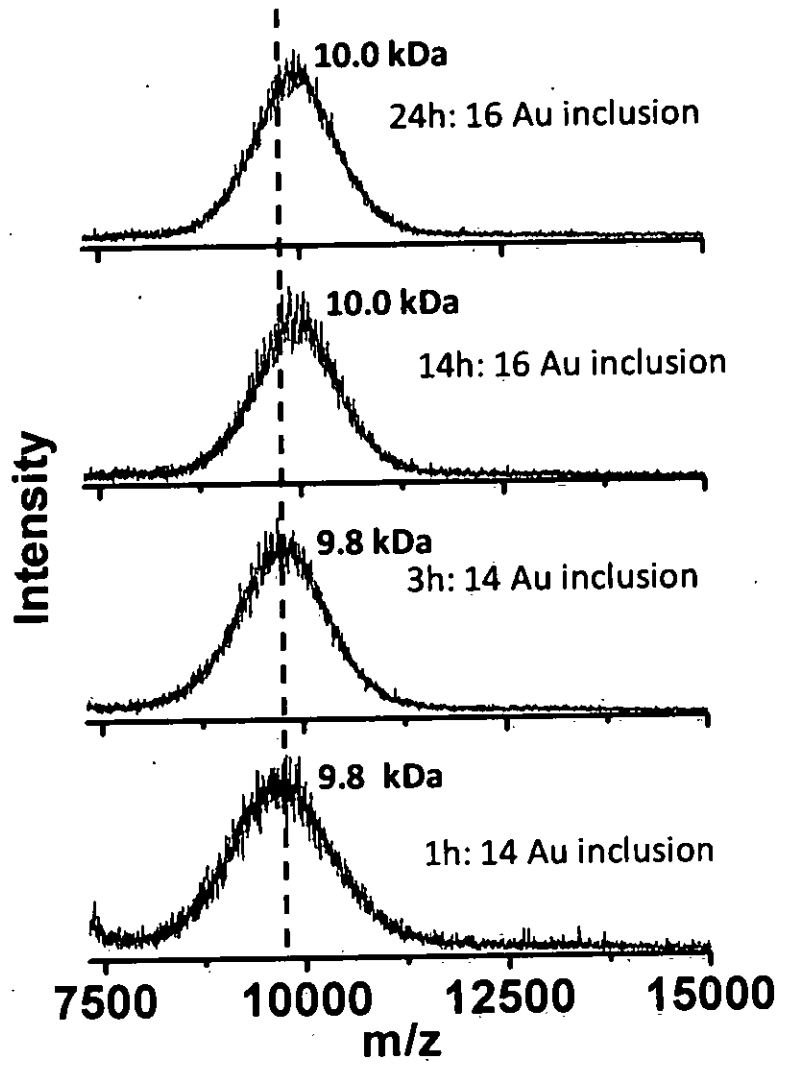

FIGURE 28

Signature:

D. Moses Jeyakaran
Advocate & Patent Agent
IN/PA — 369

METHOD OF MAKING ALLOYS OF PRECISE COMPOSITION USING INTER-CLUSTER REACTIONS IN SOLUTION

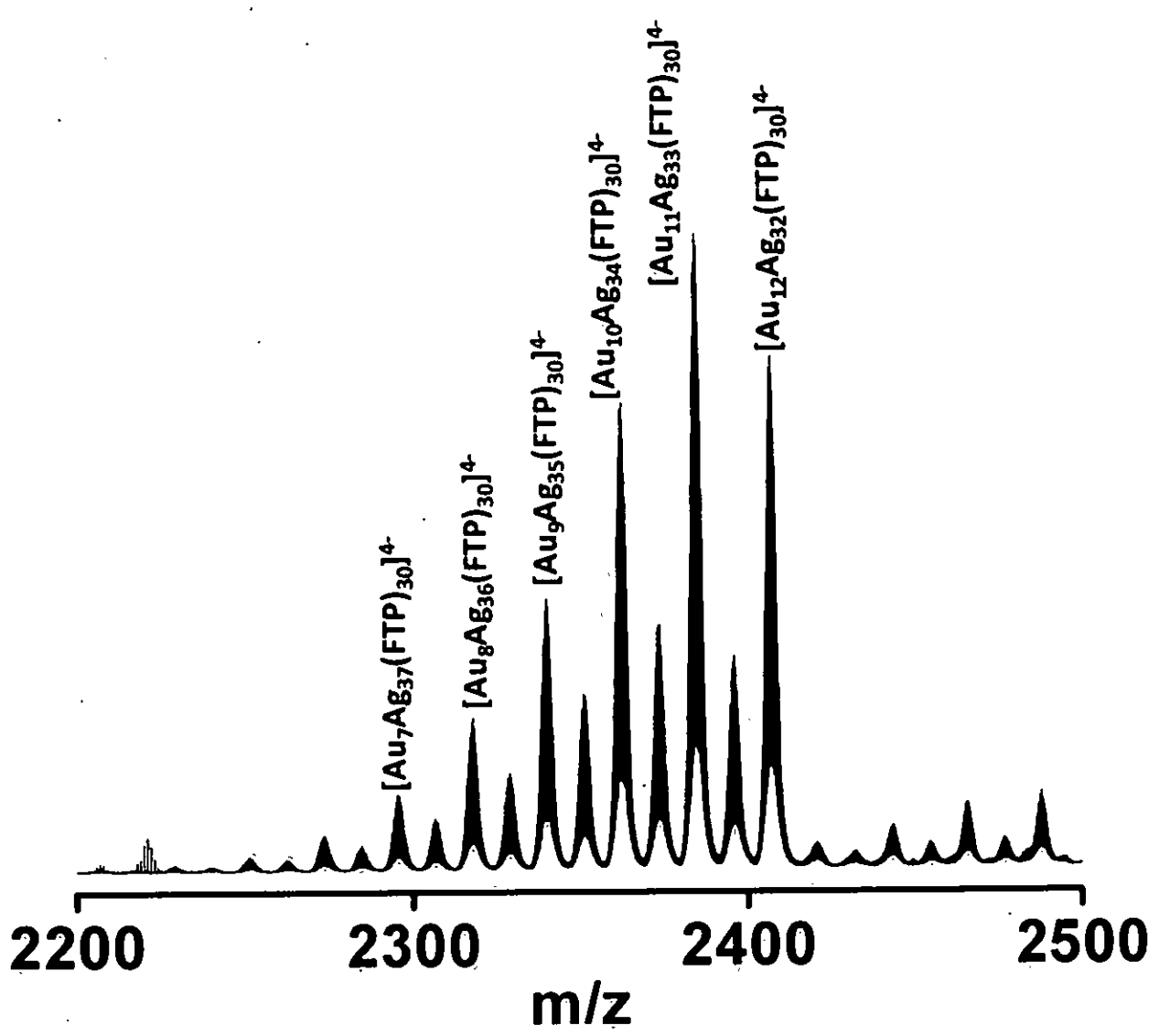

FIGURE 29

Signature:

D. Moses Jeyakaran
Advocate & Patent Agent
IN/PA — 369

METHOD OF MAKING ALLOYS OF PRECISE COMPOSITION USING INTER-CLUSTER REACTIONS IN SOLUTION

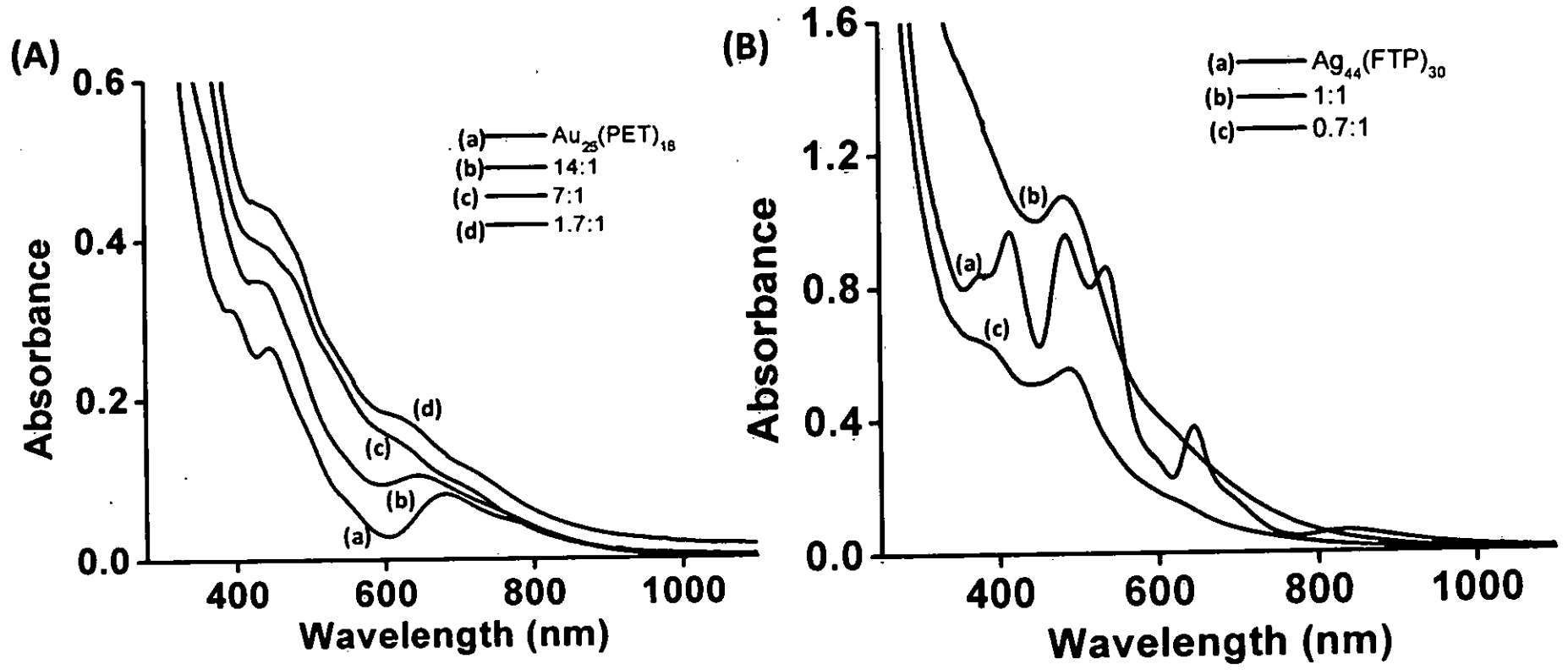

FIGURE 30

Signature:

D. Moses Jeyakaran
Advocate & Patent Agent
IN/PA — 369

METHOD OF MAKING ALLOYS OF PRECISE COMPOSITION USING INTER-CLUSTER REACTIONS IN SOLUTION

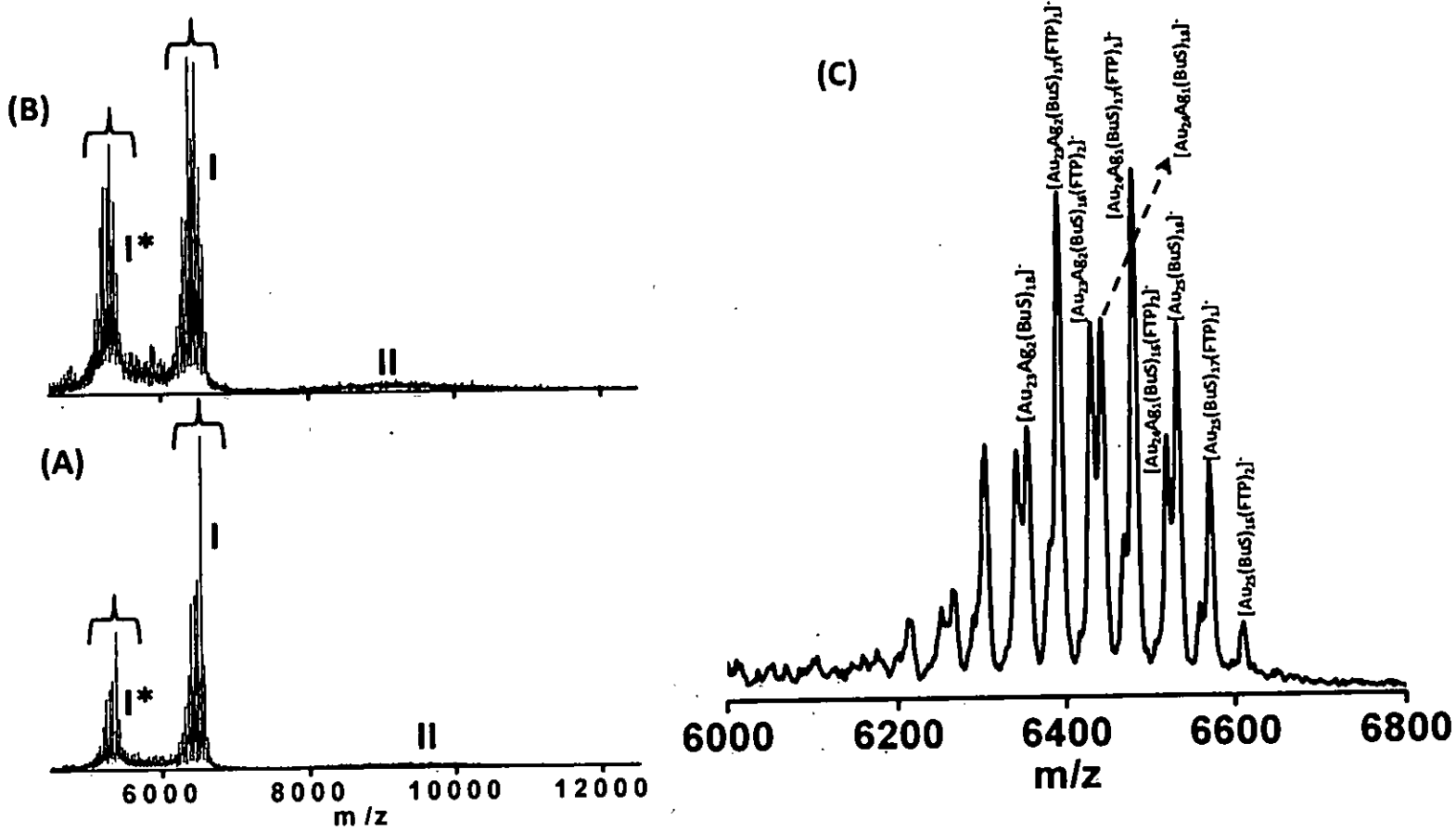

FIGURE 31

Signature:

D. Moses Jeyakaran
Advocate & Patent Agent
IN/PA — 369

METHOD OF MAKING ALLOYS OF PRECISE COMPOSITION USING INTER-CLUSTER REACTIONS IN SOLUTION

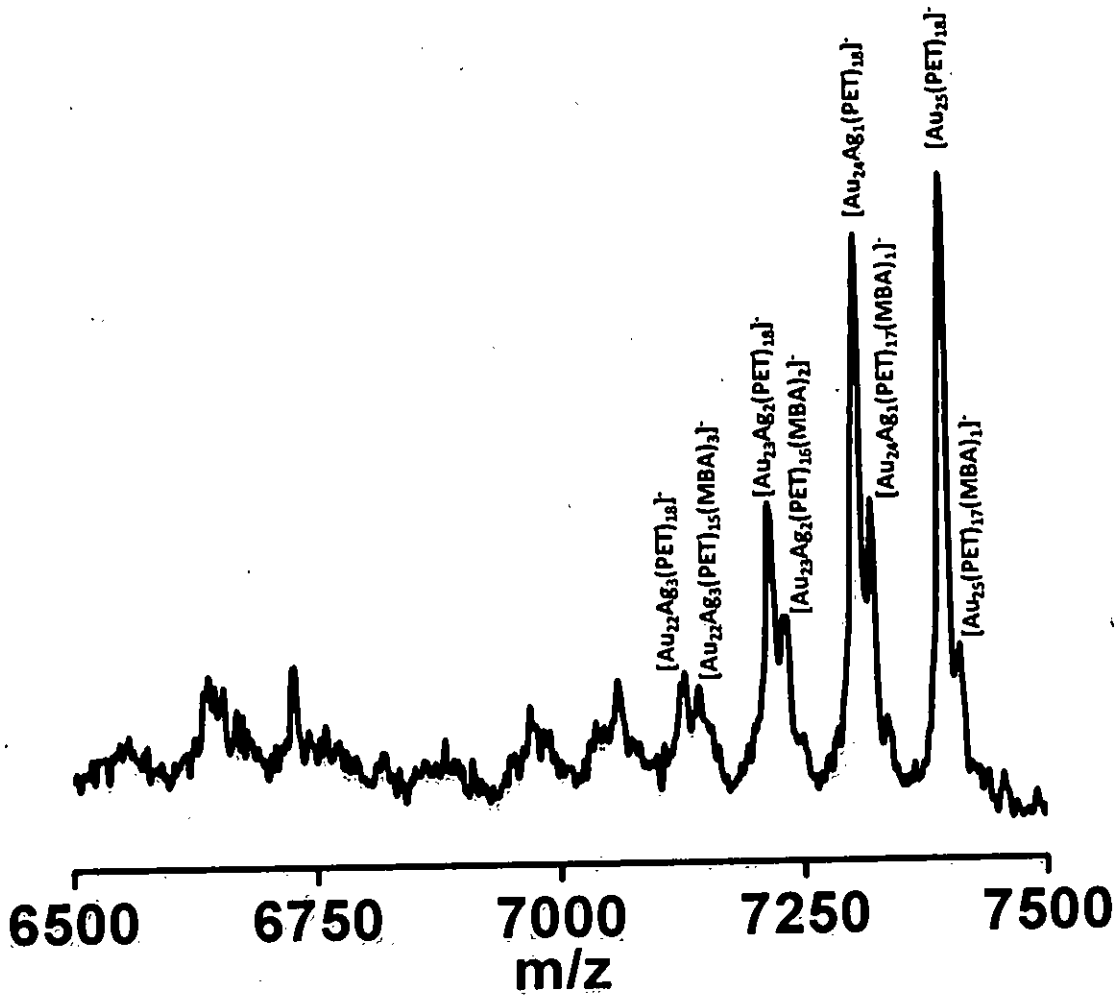

FIGURE 32

Signature:

D. Moses Jeyakaran
Advocate & Patent Agent
IN/PA — 369

METHOD OF MAKING ALLOYS OF PRECISE COMPOSITION USING INTER-CLUSTER REACTIONS IN SOLUTION

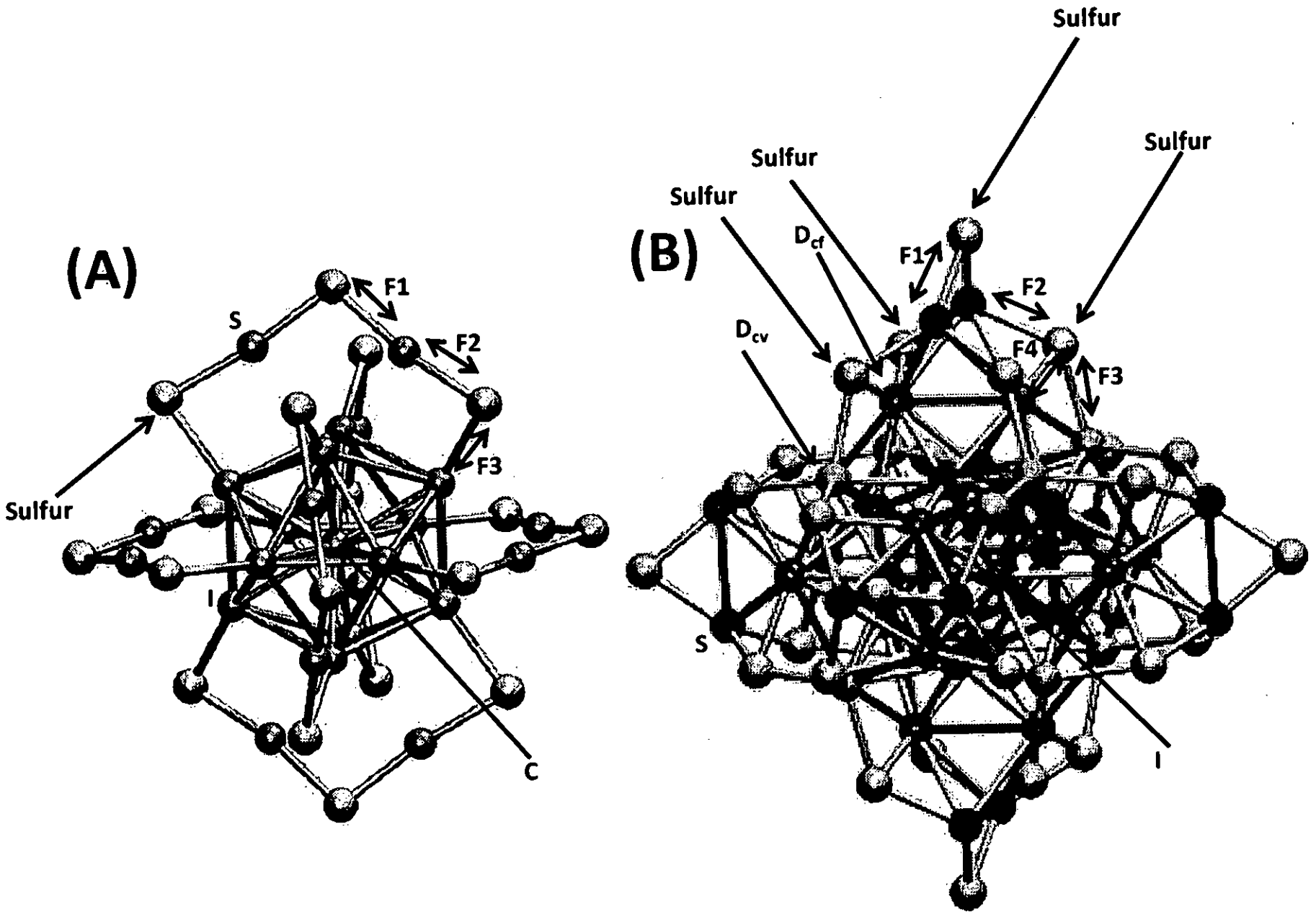

FIGURE 33

Signature:

D. Moses Jeyakaran
Advocate & Patent Agent
IN/PA — 369

METHOD OF MAKING ALLOYS OF PRECISE COMPOSITION USING INTER-CLUSTER REACTIONS IN SOLUTION

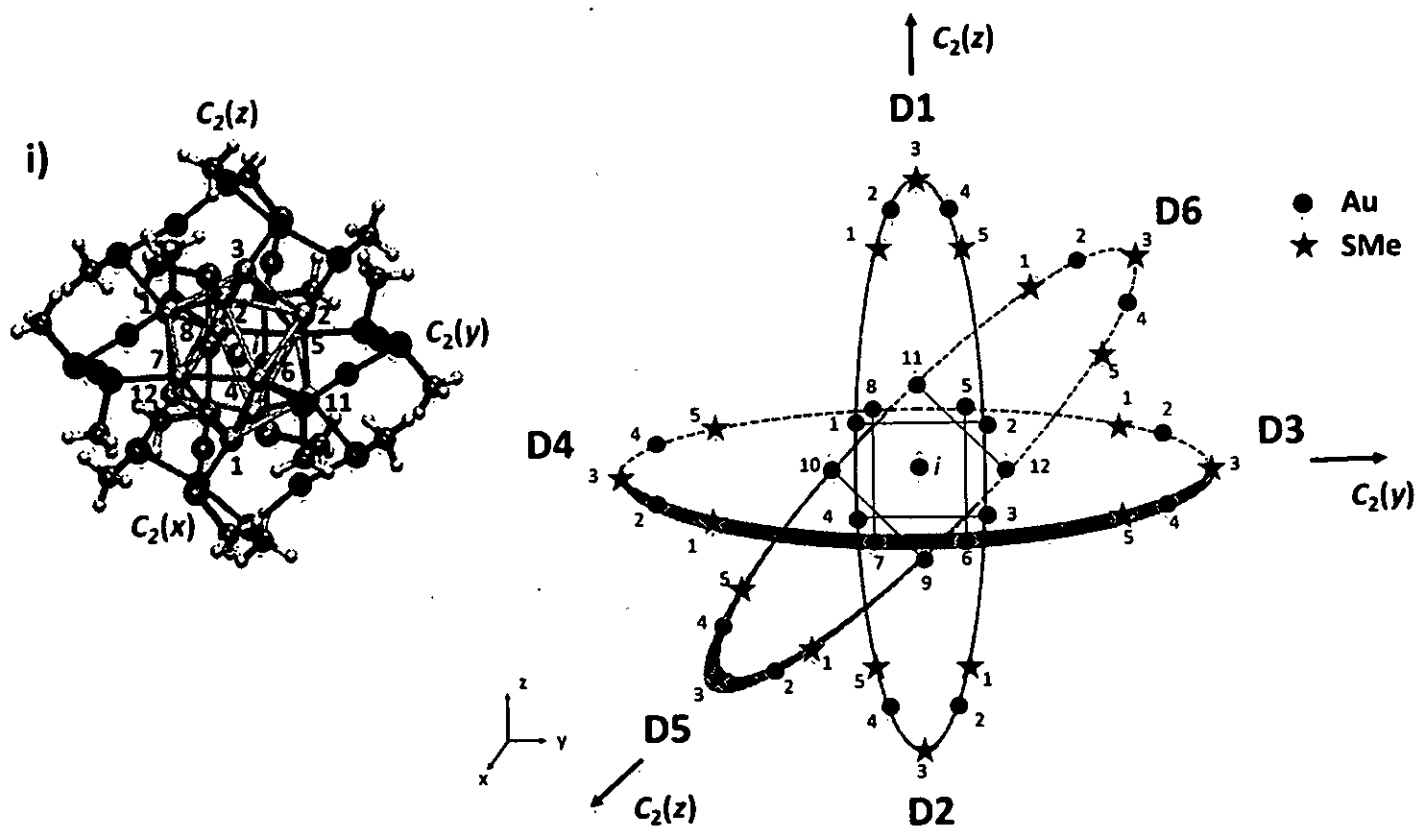

FIGURE 34

Signature:

D. Moses Jeyakaran
Advocate & Patent Agent
IN/PA — 369

METHOD OF MAKING ALLOYS OF PRECISE COMPOSITION USING INTER-CLUSTER REACTIONS IN SOLUTION

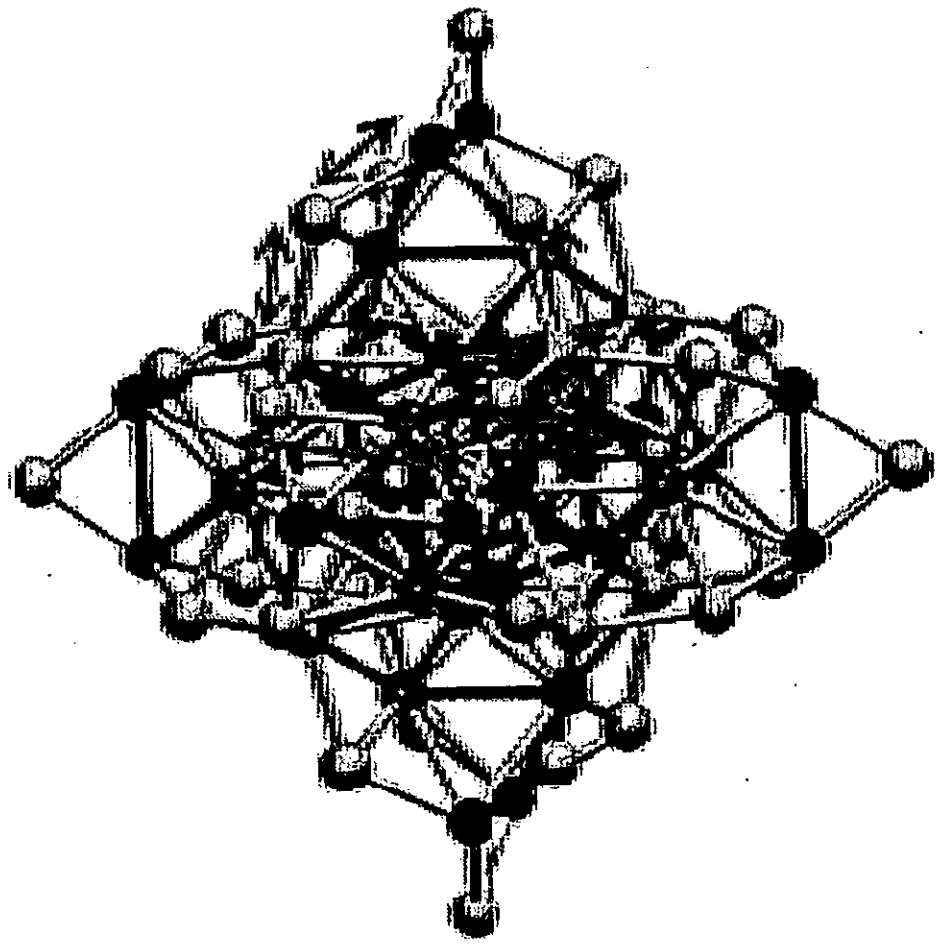

FIGURE 35

Signature:

D. Moses Jeyakaran
Advocate & Patent Agent
IN/PA — 369

METHOD OF MAKING ALLOYS OF PRECISE COMPOSITION USING INTER-CLUSTER REACTIONS IN SOLUTION

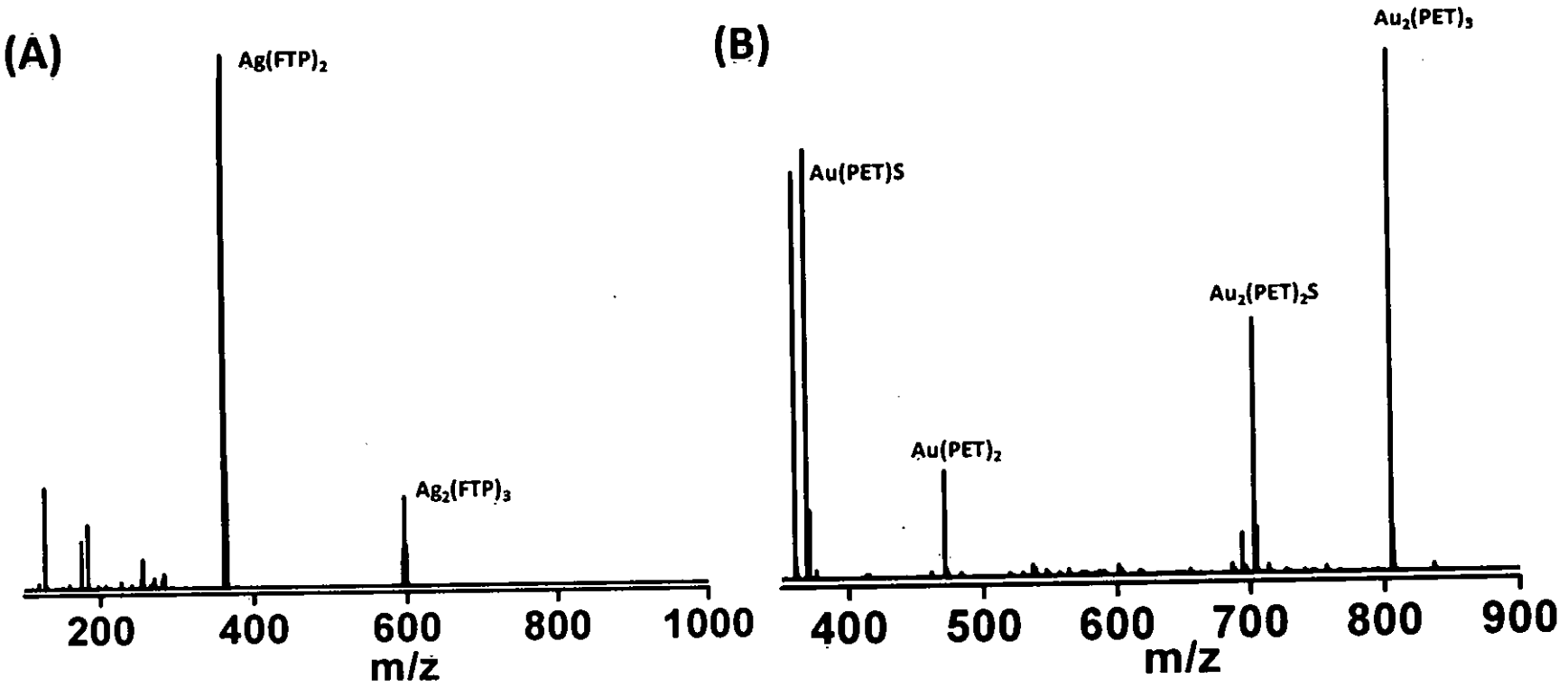

FIGURE 36

Signature:

D. Moses Jeyakaran
Advocate & Patent Agent
IN/PA — 369

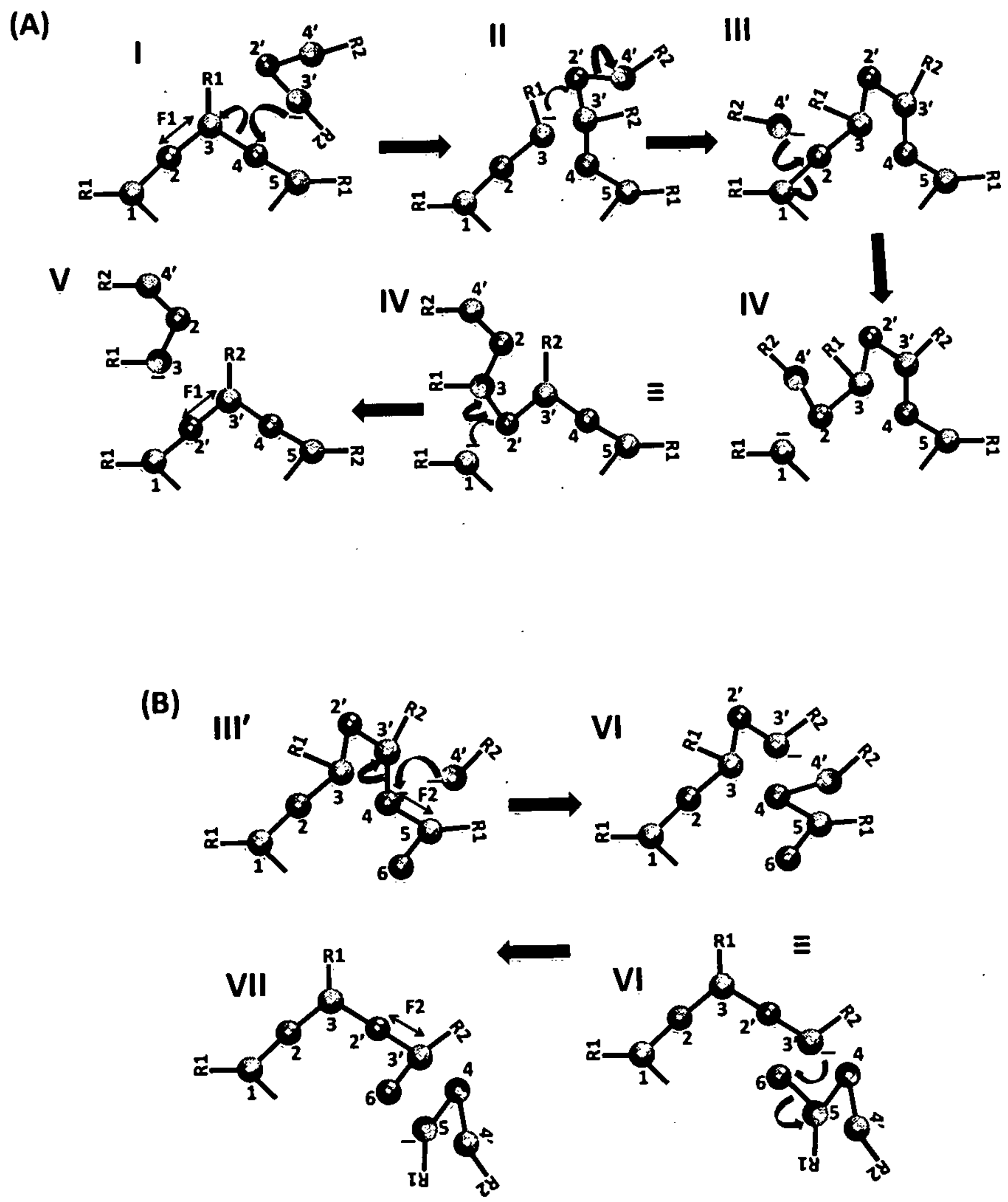

FIGURE 37

Signature:

D. Moses Jeyakaran
Advocate & Patent Agent
IN/PA — 369

METHOD OF MAKING ALLOYS OF PRECISE COMPOSITION USING INTER-CLUSTER REACTIONS IN SOLUTION

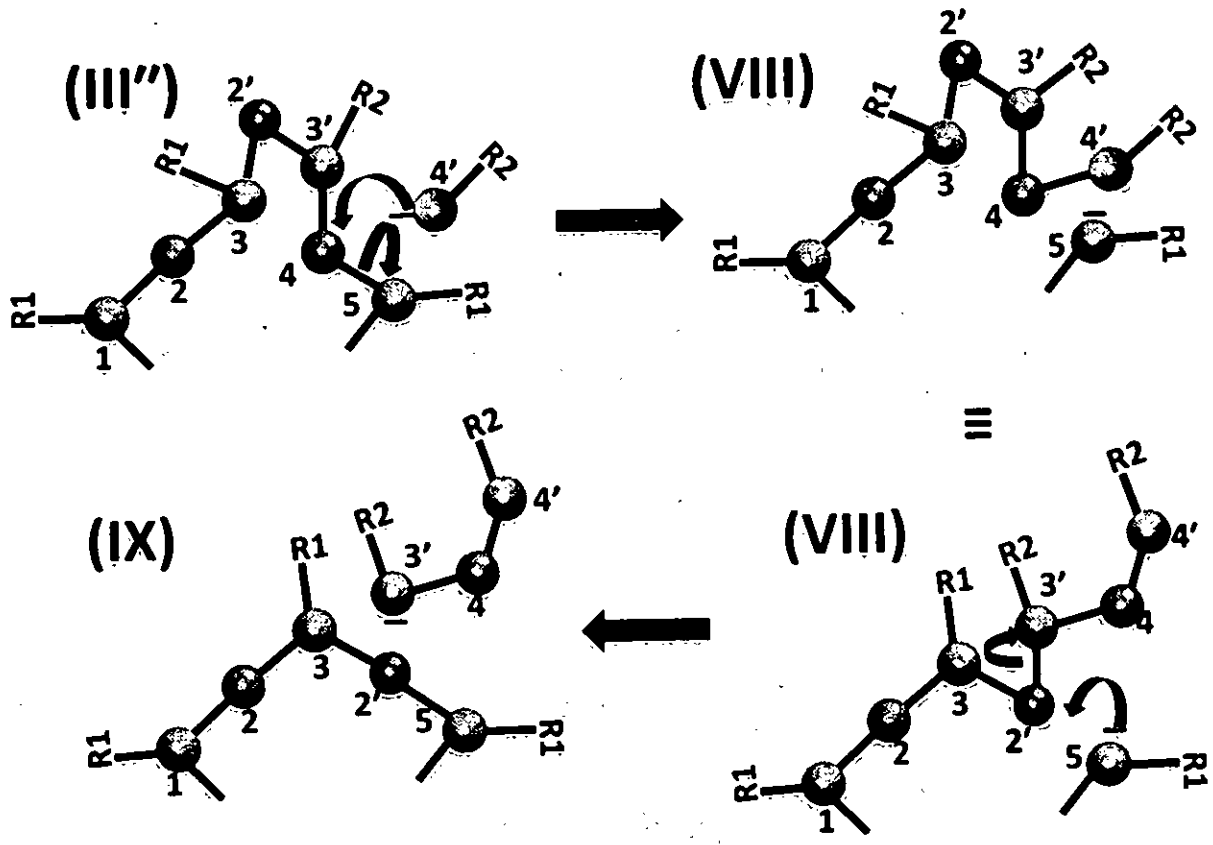

FIGURE 38

Signature:

D. Moses Jeyakaran
Advocate & Patent Agent
IN/PA — 369